Ti:Tm:$LiNbO_3$ Waveguide Amplifiers And Lasers

Thesis

Submitted to the
Department of Physics,
Faculty of Science
University of Paderborn, Germany
for the degree
Doktor der Naturwissenschaften (Dr. rer. nat.)

by

MATHEW GEORGE

REVIEWERS:
Prof. Dr. Wolfgang Sohler
Prof. Dr. Donat As
DATE OF SUBMISSION: 06.09.2012
DATE OF EXAMINATION: 02.10.2012

ABSTRACT

The fabrication of Ti:Tm:$LiNbO_3$ waveguides by diffusion doping is briefly described. The waveguides thus fabricated have been characterized by determining the propagation losses, near field intensity profile, fluorescence spectrum, absorption spectrum and Tm depth profile by secondary neutral mass spectroscopy. Emission cross sections of the gain medium Ti:Tm:$LiNbO_3$ have been determined by McCumber theory from the experimentally determined absorption cross sections. A sensitive experimental setup was developed to perform all spectral measurements. For the first time an in-band pumped (λ_p = 1650 nm)Ti:Tm:$LiNbO_3$ waveguide amplifier capable of broadband optical amplification in the spectral range 1750 nm $< \lambda_s <$ 1900 nm is demonstrated. Experimental results of small signal gain measurements were found to be in good agreement with the modeling results. Modeling results show (wavelength dependent) gain of up to 30 dB in a 10 cm long single pass pumped waveguide. A double pass pumping scheme can improve the gain achievable significantly. Fabry-Pérot type lasers (λ_s = 1890 nm and 1850 nm) have been realized by depositing specially designed mirrors at the waveguide amplifier endfaces. Laser threshold (1890 nm) is at 4 mW coupled pump power; the slope efficiency is ~13.3%. The slope efficiency (laser threshold) is larger (smaller) by more than an order of magnitude than those reported so far for Tm:$LiNbO_3$ waveguide lasers. Modeling results show that the slope efficiency can be improved to 34% by redesigning one mirror. The fabrication and characterization of Ti:Tm:$LiNbO_3$ waveguide for quantum memory applications is included as an appendix.

ZUSAMMENFASSUNG

Die Herstellung von Ti:Tm:$LiNbO_3$ Wellenleitern durch Diffusionsdotierung wird kurz beschrieben. Die so hergestellten Wellenleiter wurden sehr genau mit verschiedenen Methoden experimentell untersucht, um Ausbreitungsverluste, Nahfeldverteilungen, Fluoreszenzspektren, Absorptionsspektren und Tm-Tiefenprofile zu bestimmen. Die Emissionswirkungsquerschnitte des Verstärkungsmediums Ti:Tm:$LiNbO_3$ wurden mit Hilfe der McCumber Theorie aus den experimentell ermittelten Absorptionsquerschnitten berechnet.

Ein experimenteller Aufbau zur Durchführung äußerst empfindlicher spektraler Messungen wurde entwickelt. Zum ersten Mal gelang es, breitbandige Verstärkung mit 'in-band'-gepumpten (λ_p = 1650 nm) Ti:Tm:Li:NbO_3 Wellenleitern im Wellenlängenbereich

1750 nm $< \lambda_s <$ 1900 nm zu erhalten. Die experimentell bestimmte Kleinsignalverstärkung dieser Wellenleiterverstärker ist in guter Übereinstimmung mit Modellierungsergebnissen. Weitere Rechenergebnisse sagen eine (wellenlängenabhängige) Verstärkung von bis zu 30 dB in einem 10 cm langen Wellenleiter voraus. Mit einer 'double-pass' Pumpanordnung kann die optische Verstärkung weiter deutlich verbessert werden.

Durch Aufdampfen speziell entwickelter Spiegelschichten auf die Wellenleiterendflächen wurden Laser vom Fabry-Pérot Typ hergestellt mit Emissionswellenlängen von 1890 nm (Resonator hoher Güte) und 1850 nm (Resonator geringerer Güte). Die Laserschwelle (λ_s = 1890 nm) beträgt 4 mW eingekoppelter Pumpleistung; die 'slope efficiency' ist 13.3%. Damit sind beide Werte um mehr als eine Größenordnung größer ('slope efficiency') bzw. kleiner (Laserschwelle) als entsprechende Ergebnisse, die bisher zu Tm:$LiNbO_3$ Wellenleiterlasern veröffentlicht wurden. Weitere Modellierungsergebnisse zeigen, dass die 'slope efficiency' bis zu 34% erhöht werden kann, wenn die Resonatorspiegel optimiert werden.

Die Herstellung und Charakterisierung von Ti:Tm:LiNbO3 Wellenleiter für Anwendungen als Quantenspeicher werden im Anhang diskutiert.

CONTENTS

1 INTRODUCTION

1.1 BACKGROUND

Lasers are sources of coherent, diffraction limited electromagnetic beams. The acronym *laser* (light amplification by stimulated emission of radiation) is based on the fact that lasers rely on the phenomenon called stimulated emission of radiation for amplification of light. When reported for the first time by Maiman [1] in 1960, its critics described lasers as *a solution looking for a problem*. Now, more than five decades after that remarkable invention, lasers find applications in day to day life in devices like CD players, bar code scanners etc. and in a variety of fields, like communications, metrology [2], medicine [3], etc. to name a few.

Integrated optics refers to the integration of various optical devices like lasers, modulators, beam splitters etc. into one substrate [4]. Its essential feature is the fabrication of multifunctional chips, like in the case of integrated circuits in the domain of electronics. Four decades after the first proposal [5] of integrated optics, a lot of progress has been made in fabricating various devices as well as in the integration of several devices in one chip [6]. Integrated lasers have improved properties in comparison to their bulk counter-parts [7] due to (i) the reduction of cavity mode volume due to optical confinement, (ii) higher optical gain, (iii) lower thresholds and (iv) the possibility for integrating several devices (including the laser) in one chip.

Lithium niobate ($LiNbO_3$) is a versatile substrate for integrated optics because of its excellent electro-optic, acousto-optic, nonlinear optic properties combined with the possibility to fabricate low loss optical waveguides [8]. Moreover, it can be easily doped with rare-earth ions (to get a laser active material and) to take advantage of the favorable properties of both, the host material and the rare earth ions simultaneously. A prominent example is the demonstration of a whole family of erbium doped waveguide lasers namely Fabry-Pèrot type lasers, Distributed Bragg Reflector- (DBR-) lasers, acousto-optically tunable lasers, electro-optically Q-switched lasers and harmonically mode-locked lasers [9] and of neodymium doped waveguide lasers [10, 11]. Also attractive properties of rare earth-doped waveguide amplifiers in $LiNbO_3$ have been shown [11, 12]. Another more recent example is the demonstration of a thulium-doped waveguide quantum memory in $LiNbO_3$ [13].

The research presented in this thesis started with the discovery of self-pulsations from a Fabry-Pérot type Ti:Er:$LiNbO_3$ waveguide laser (λ_p= 1480 nm, λ_s= 1611 nm) [14]. The laser was found to emit pulses, as in the case of a passively mode locked laser, without the aid of any intracavity elements to induce such pulsations. This observation immediately raised several open questions.

Would it make any difference if the laser active ions are different? In order to find the answer, Ti:Tm:$LiNbO_3$ waveguide amplifier and subsequently lasers were developed. This is described in detail in this thesis. Although the answer to the question posed above seems to be *no* as hinted by the laser results, it is yet to be proved beyond doubt.

Apart from the academic interests which motivated this research there are other equally interesting aspects from the point of view of applications of the integrated lasers mentioned above. Lasers operating at wavelengths longer than 1380 nm are termed *eye safe*. This is because of the strong absorption of these wavelengths by the front part of the human eye (cornea and vitreous humor) resulting in some sort of protection[1] to the retina [15]. There are several applications where such eye safe lasers are needed because the radiation cannot be guided. Laser radar, remote sensing, communications etc. are examples of such applications. In particular Tm-doped lasers, depending on the host material, emit in the wavelength range 1650 nm to beyond 2000 nm. Two example applications of Tm lasers are mentioned in the following. Several gas molecules have absorption bands falling in this spectral region. Tm-doped lasers can be used for the spectroscopy and detection of such gases. Tm lasers emitting at the appropriate wavelength can be used for performing laser surgery. This is because of the strong water absorption lines falling in the emission spectrum of Tm.

There is a growing interest in Tm-doped $LiNbO_3$ waveguide lasers utilizing the $^3F_4 \rightarrow {}^3H_6$ transition to get emission in the wavelength range 1600 nm $< \lambda <$ 1900 nm [16, 17] and in Tm-doped waveguide lasers in other hosts [18, 19]. Up to now, Tm:$LiNbO_3$ lasers were pumped at 795 nm wavelength exploiting the strong absorption by the $^3H_6 \rightarrow {}^3H_4$ transition. This thesis discusses the development of in-band pumped (λ_p= 1650 nm) Ti:Tm:$LiNbO_3$ waveguide amplifiers and Fabry-Pérot type Ti:Tm:$LiNbO_3$ waveguide lasers (λ_s= 1890 nm and 1850 nm).

1 This applies only to stray radiations of low powers. With high power radiation adequate saftey measures should be taken.

The core component of the waveguide amplifiers and laser cavities mentioned in this thesis is a Ti:Tm:$LiNbO_3$ waveguide. The fabrication of Ti:Tm:$LiNbO_3$ waveguides and their characterization are mentioned in chapter 2. Chapter 3 discusses how a Ti:Tm:$LiNbO_3$ waveguide can be used as an amplifier. An in-band pumped Ti:Tm:$LiNbO_3$ waveguide amplifier capable of achieving broadband optical gain in the wavelength range 1750 nm $< \lambda <$ 1900 nm is demonstrated. This chapter includes a discussion of in-band pumping, extensive modeling of amplifiers, the specially developed experimental setup for small signal gain measurements, results of small signal gain measurements which are in good agreement with modeling results and a discussion on amplifiers for laser applications. The waveguide lasers operating near 1890 nm and 1850 nm developed using a Ti:Tm:$LiNbO_3$ waveguide amplifier is presented in chapter 4. This chapter includes a discussion of the formation of laser cavity, results of laser experiments done with both lasers and optimization of the 1890 nm laser. The highlight is the first demonstration of an in-band pumped Ti:Tm:$LiNbO_3$ waveguide laser (i) emitting at the longest emission wavelength, (ii) with the smallest laser threshold and the highest output power reported from a Tm:$LiNbO_3$ waveguide laser, so far.

A Ti:Tm:$LiNbO_3$ waveguide can be used as a solid state quantum memory [13]. Appendix A briefly outlines the fabrication and characterization of Ti:Tm:$LiNbO_3$ waveguides for quantum memory applications.

2

WAVEGUIDE FABRICATION AND CHARACTERIZATION

2.1 INTRODUCTION

By doping lithium niobate (LN) with rare earth (RE) ions, it is possible to fabricate integrated optical devices which make use of the properties of the host material as well as the rare earth ion. RE doped integrated lasers [20, 10] in LN are examples of such devices where the possibility to fabricate low loss waveguides in LN is combined with the laser properties of the rare earth ion. The laser(s) described in this thesis were fabricated by three processing steps: (i) indiffusing the RE ion (Er or Tm) into congruent lithium niobate (CLN), (ii) formation of Ti indiffused waveguides fabricated on the RE doped surface and (ii) subsequently the laser cavity was formed by coating suitable mirrors on waveguide endfaces.

Laser active ions can be incorporated into LN lattice by various techniques. For example Er can be doped into LN lattice by indiffusion, ion implantation, pulsed laser deposition or by growing the crystal from a doped melt [21]. Our group has performed Pr doping [22] and Er doping [20, 9] in the past as well as Tm doping [23, 24] of LN by indiffusion recently. Particularly, detailed investigations on diffusion doping of Er were done and the results are described in [21]. Irrespective of the dopant used, we start by coating a planar layer of the RE atoms on the surface of a CLN wafer. Due to the lithium deficiency (Li/Nb=0.94) in CLN, the dopant atoms occupy regular lattice sites and a dopant concentration of several mole % can be realized. Afterwards, this layer is indiffused at a temperature lower than the Curie temperature of LN (1140 ^{0}C), so that the ferro electric phase of the lattice is not disturbed during the diffusion process.

In this chapter a brief overview on RE doping of LN by indiffusion (with Tm-doping as an example), subsequent Ti waveguide fabrication and the characterization of the fabricated waveguides thus formed are given.

2.2 FABRICATION OF TI:TM:$LINBO_3$ WAVEGUIDE

The RE doped waveguides (and laser cavities) used for the research mentioned in this thesis were fabricated by Raimund Ricken and Viktor Quiring from the technology wing of our lab.

2.2.1 *Tm Diffusion Doping*

Fig. 2.1 depicts the different steps of waveguide fabrication which were discussed above. Commercially available 0.5 mm thick Z-cut wafer of undoped optical grade CLN were Tm-doped near the +Z-surface before waveguide fabrication. A vacuum deposited Tm layer of 32 nm thickness was in-diffused at 1130 ^{0}C during 150 hours in an argon atmosphere followed by a post treatment in oxygen (1 hour).

2.2.2 *Fabrication of Ti Waveguide*

On the Tm-doped surface 104 nm thick Ti layer was deposited first. Subsequently stripes with widths ranging from 4.5 µm to 8.5 µm in steps of 0.5 µm were defined by a photolithography step and in-diffused at 1060 ^{0}C for 9.6 hours to form 60 mm long optical strip waveguides. Subfigure 6 of Fig. 2.1 shows the co-ordinate system of the crystal (capitals) with respect to the laboratory frame (small letters).

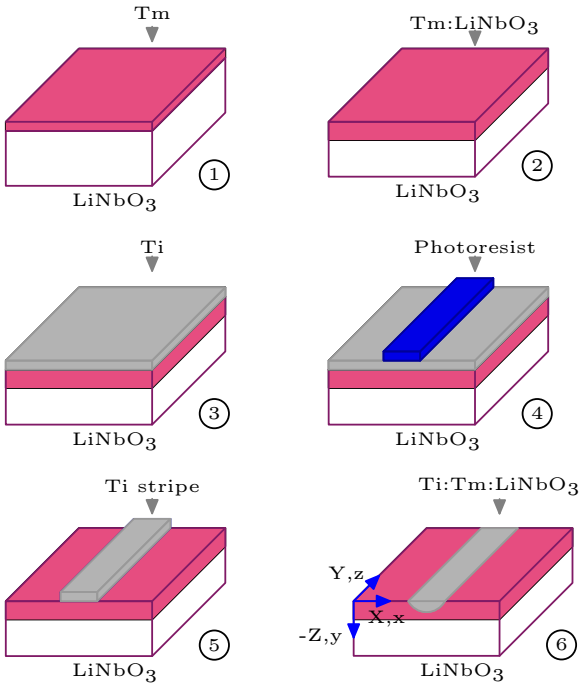

Figure 2.1: Ti:Tm:$LiNbO_3$ waveguide fabrication steps. 1 & 2 - Tm deposition and indiffusion, 3 - Ti deposition, 4 & 5 Ti stripe defenition and 6 - Ti indiffusion to realize Ti:Tm:$LiNbO_3$ waveguide.

The thickness of the RE layer, the diffusion temperature and the indiffusion time are adjusted in such a way that the (i) resultant RE depth profile has a good overlap with the fundamental waveguide mode of both pump and signal emissions as well as (ii) the reservoir (RE layer) is completely depleted resulting in a smooth surface which is essential for the realization of low loss optical waveguides. The

thickness of the Ti layer, the diffusion temperature and the indiffusion time are adjusted in such a way that the waveguides are mono mode for wavelengths larger than 1500 nm. Indiffusion of RE ions is done prior to the fabrication of Ti waveguides. This is due to the fact that the Ti indiffusion occurs at a much faster rate in comparison to the RE indiffusion.

Afterwards, the sample was cut to 5 mm, 10 mm, 15 mm and 30 mm long pieces (breadth = 12 mm, in all cases) and the end faces of each piece were polished perpendicular to the waveguides. The 15 mm long sample was used for investigations to determine waveguide properties, except for the fluorescence measurement which was done with the 5 mm long sample. Subsequently, the 15 mm long sample was used for amplifier experiments and the 30 mm long sample was used for laser (fabrication and) experiments. The width of the waveguide which was used for both amplifier and laser experiments is 6.5 μm.

2.3 CHARACTERIZATION OF Ti:Tm:$LiNbO_3$ WAVEGUIDE

The various properties of the waveguide namely, mode intensity distribution, scattering loss, Tm doping profile, absorption spectrum, fuorescence spectrum and transition cross sections were characterized as mentioned below.

2.3.1 *Waveguide Mode Intensity Distribution*

Whether the waveguide is monomode as designed can be tested by measuring the near field intensity distributions. The near field intensity distribution of the waveguide mode was measured by imaging the magnified (100x) waveguide mode onto an infrared camera. Amplified spontaneous emission from a 1650 nm diode laser operated below threshold was used as the light source for this measurement so as to minimze the potential errors that could arise from interference effects. From the captured image (see Fig. 2.2) the dimensions of the intensity profile is calculated using a specially developed software[1]. The measured full width at half maximum of the fundamental TE mode at 1650 nm is 7.8 μm × 6.2 μm. On the other hand the calculated FWHM of the TE mode at 1650 nm, with fabrication parameters of Pb304z input to Focus [25] are 7.0 μm × 5.2 μm. This is slightly smaller in comparison with the measured values. The software takes the bulk density of Ti for performing the calculation whereas the actual density is slightly lower. This is the reason for the discrepancy.

1 by Dr.Ansgar Hellwig.

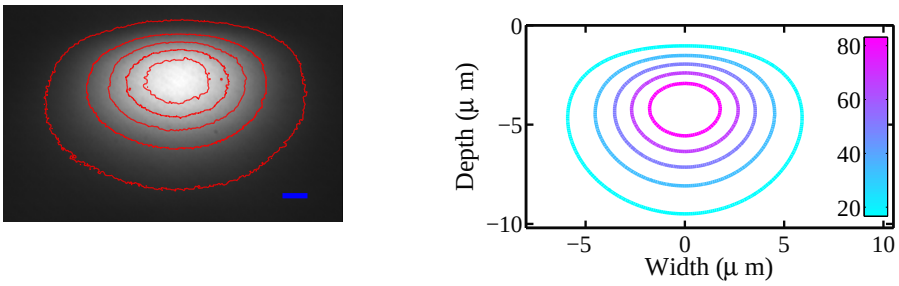

Figure 2.2: Measured (left) and calculated (right) mode intensity profiles of a 6.5 μm waveguide. The blue line (in measurement data) corresponds to 1 μm. Isolines are drawn at intensity levels corresponding to 90%,70%,50% etc.

2.3.2 *Scattering Losses*

The propagation losses of Ti:Tm:LN waveguides were measured by the Fabry-Pérot method which was developed in our group [26]. A waveguide with polished endfaces perpendicular to the waveguide itself form a low finesse Fabry-Pérot resonator because of the residual endface reflectivities arising from the air:LN interface. During the experiment the transmitted optical power behind such a waveguide resonator is measured as a function of wavelength (or as a function of the resonator length) using the setup shown in Fig.2.3. A narrow band laser emission with a coherence length longer than twice the optical path length of the waveguide is used as the light source in the experiment so that the Fabry-Pérot resonances of the low finesse cavity can be measured. From the measured curve (see actual measurement data in Fig.2.4), we can calculate the waveguide propagation losses with the following relation,

$$\alpha = \frac{4.34}{L}(\ln[R] + \ln[2] - \ln[K]) \tag{2.1}$$

where the contrast, $K = \frac{I_{max}-I_{min}}{I_{max}+I_{min}}$, R is the waveguide endface reflectivity and L is the length of the waveguide in cm. With the above expression α is obtained in units of dB/cm.

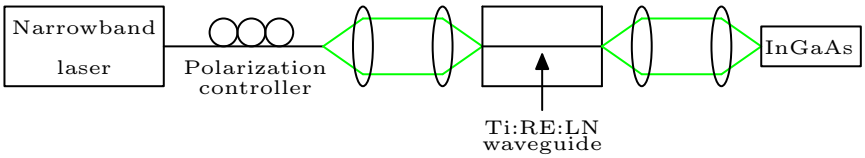

Figure 2.3: Experimental setup used to measure waveguide propagation loss.

Narrow band emission centered at 1505 nm (from a tunable extended cavity diode laser) was used for the measurement because of (i) the weak Tm absorption at this wavelength and (ii) the fact that only the fundamental mode will be supported by the waveguide. Apart from the 6.5 μm waveguide, the adjacent 7 μm waveguide was also used for the measurement. The result from the 7 μm waveguide for TE polarised light is shown in Fig.2.4. For this result,

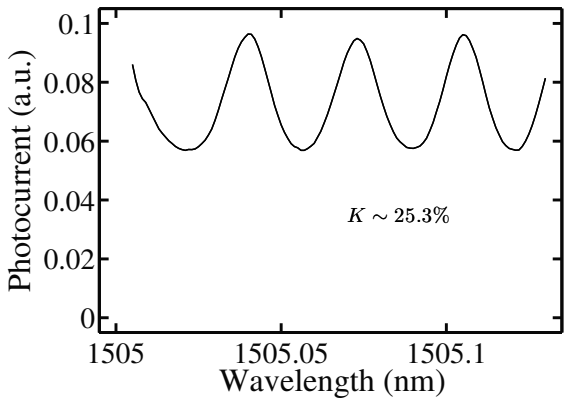

Figure 2.4: Measured Fabry-Pérot resonances from a Tm-doped 7 μm wide waveguide (l=15 mm).

the calculated scattering loss value is 0.3 dB/cm. In the case of a 6.5 μm waveguide, the measured scattering loss value is slightly higher (0.4 dB/cm). On the other hand for an undoped (i.e., without Tm) 7 μm wide waveguide the scattering loss value is only 0.2 dB/cm. The difference of the scattering losses could be due to surface roughness arising from the Tm doping. One of the parameters that needs to be input for laser modeling is the propagation loss of the waveguide. It was observed that the calculated power characteristics (see section 4.4) agrees reasonably well with the measured result, when the scattering loss value is only 0.1 dB/cm. Hence, the measured result could be slightly higher than the actual scattering losses of the 6.5 μm waveguide.

2.3.3 *Thulium Depth Profile*

The doping profile of Tm ions was measured by secondary neutral mass spectroscopy (SNMS). The measurement was performed (by Dr.Huberus Paulus from Fachhochschule Südwestfalen, Söest.) using 700 eV Argon-ions for ion milling. Ions and electrons were extracted from the plasma source with a duty cycle of 4:1 at a rate of 320 kHz to avoid charging of the insulating CLN-substrate. SNMS was chosen instead of secondary ion mass spectroscopy (SIMS) to significantly reduce matrix effects (see e.g. [27]). In Fig. 2.5, the concentration profile versus depth has been recorded for thulium (Tm). It is expected that

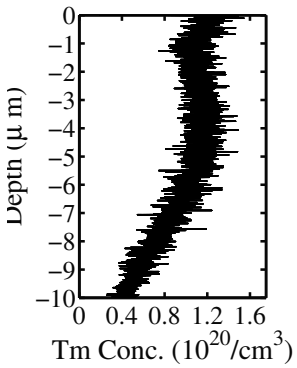

Figure 2.5: Measured Tm depth profile.

Tm occupies regular Li-sites similar to Er-ions when incorporated in CLN by diffusion [28]. The maximum Tm concentration (at surface) of the sample was about $1.25\times10^{20}cm^{-3}$ corresponds to a concentration 0.68 mole % and a penetration depth ($d_{1/e}$) of 9 microns.

Thulium (^{69}Tm) is the 13^{th} element in the lanthanide series with the electronic configuration - $[Xe]4f^{13}6s^2$. In pure form it is a soft metal. Upon incorporation into a dielectric host, it loses three electrons to become $[Xe]4f^{12}$ (or Tm^{3+}). The unfilled 4f electrons interact by spin-spin and spin-orbit interaction and this leads to different energy levels among the 4f electrons. As an example, the $^3H_6$, $^3H_4$ and $^3F_4$ energy levels of a Tm ion in LN lattice along with different transitions resulting from absorption or emission of photons are shown in Fig. 2.6 (left). When incorporated into a host, the crystal field lifts the degeneracy of the different energy levels leading to a spread in energies. The corresponding splitting of $^3H_6$ and $^3F_4$ energy levels for a Tm ion incorporated into a LN lattice is shown on the right side of Fig. 2.6. These energy levels of Tm^{3+} ion are exploited from the point of view of amplifier and laser applications which are discussed in this thesis. Tm energy levels can be exploited for quantum memory applications, as well.

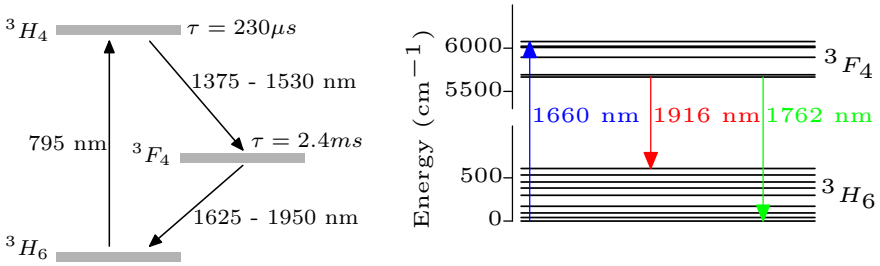

Figure 2.6: Tm:$LiNbO_3$ energy levels (from [29]) and the various transitions between them. The splitting of $^3H_6$ and $^3F_4$ energy levels is shown in the right side.

2.3.4 *Absorption Spectra*

As the next step both TE and TM polarized absorption spectra in the wavelength range 1600 nm <λ <1900 nm. were measured. This correspond to weak excitation of Tm ions from the $^3H_6$ level to the $^3F_4$ level (see Fig. 2.6).

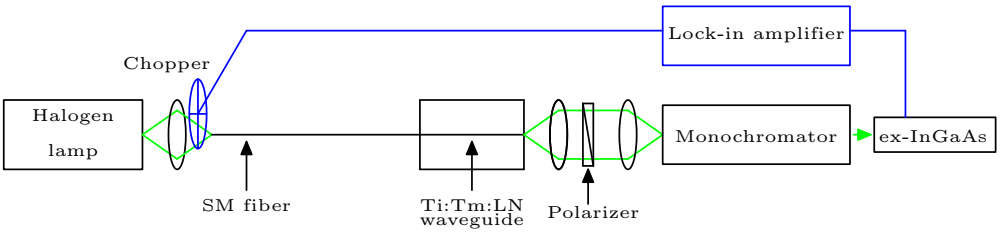

Figure 2.7: Schematic of the experimental setup developed to measure the absorption spectrum of the Ti:Tm:$LiNbO_3$ waveguide.

The schematic of the experimental setup used is shown in Fig. 2.7. A halogen lamp was used as the light source. The filament was imaged onto the end face of a standard single mode fiber (SMF 28) and the other fiber end was kept butt coupled to one endface of the waveguide. In order to avoid any Fabry-Pérot etalon effects that might arise, index matching fluid was applied at the interface. The collimated beam from behind the waveguide was analysed using a monochromator. A polarizer kept in front of the monochromator blocked the orthogonal polarisation. As the detected optical power levels were quite low, a lock-in amplifier together with a cooled extended InGaAs photodiode were used in the detection circuit. The reference signal was derived from a chopper kept in the beam behind the sample. The measurements were controlled by a computer which also recorded the data. To evaluate Tm absorption, two measurements were performed, one with a doped and the second with an undoped waveguide. The measurements were done with a resolution bandwidth of 2 nm. From published data [30] it was known that at wavelengths beyond 1950 nm Tm ions in lithium niobate have negligible absorption. Ideally both measured curves should overlap well in the spectral regions without Tm absorption (assuming identical scattering losses in both waveguides). But this was found to be a bit hard to be achieved in practice (this could be due to the fact that coupling efficiency into both doped and undoped waveguides might not be the same for the entire spectral range). In order to take care of the level differences in the measurement data (from doped and undoped waveguides) at the long wavelength side, one of the data set was multiplied by a suitable constant such that both curves overlap well at wavelengths beyond 1950 nm. Afterwards the absorption by the Tm ions was calculated by dividing the measured curve from doped waveguide and that obtained from an undoped waveguide. The results are shown in Fig. 2.8. There are two absorption bands one centered at 1660 nm and the sec-

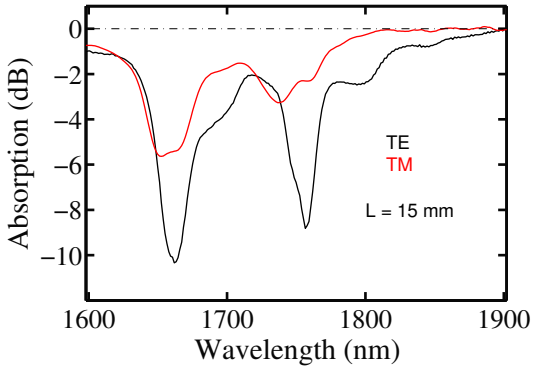

Figure 2.8: TE and TM polarised absorption spectra of a Ti:Tm:$LiNbO_3$ waveguide corresponding to $^3H_6 \rightarrow {}^3F_4$ transition in the wavelength range 1600 nm $< \lambda <$ 1900 nm. The measurement was done with a resolution bandwidth of 2 nm.

ond one at 1758 nm. The fine structure (which one might expect from the energy levels shown in Fig. 2.6) is not visible in this measurement as this measurement was done at room temperature.

2.3.5 *Fluorescence Spectrum*

TE polarised fluorescence measurement was done by pumping the waveguide with TE polarised laser light at 795 nm from a Ti:Sa (titanium sapphire) laser (see Fig.2.6 for the corresponding optical transitions). The Tm ions are excited to the $^3F_4$ level from where they subsequently relax to the $^3H_6$ level by emitting a photon (radiative transition. There could be nonradiative transitions also). For this measurement, the setup was slightly modified from what is shown in Fig. 2.7. The pump beam was coupled into the waveguide (l = 5 mm) using free space optics. The signal emitted by the sample was coupled into a PM (polarization maintaining) fiber kept butt coupled and aligned with its slow axis in the vertical direction. The other end of the fiber was aligned with its slow axis in vertical direction at the input side of the monochromator. A lens kept behind the fiber end face collimated the beam directed into the monochromator optics. A pump blocking filter kept in the free space beam path attenuated the residual pump emission from behind the waveguide. As in the absorption measurement, the measurement was done with a lock-in amplifier. The chopper was placed in the collimated beam path. The measured result is shown in Fig. 2.9. A similar measurement done by placing the chopper in the pump beam path also yielded the same result. The three prominent fluorescence peaks recorded by Cantelar [30] at 1762, 1800 and 1850 nm from bulk Tm:$LiNbO_3$ are observed in this measurement as well. These peaks also correspond to the integrated laser wavelengths reported from Tm:$LiNbO_3$ so far and these are in-

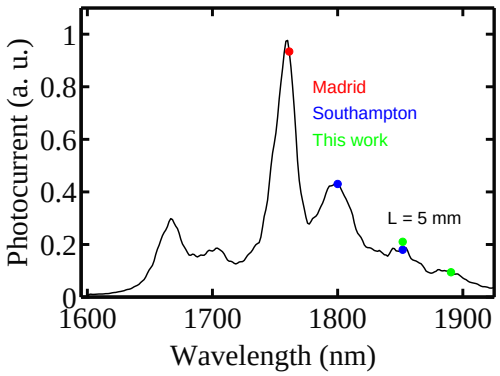

Figure 2.9: TE polarised fluorescence spectrum of a Ti:Tm:$LiNbO_3$ waveguide corresponding to $^3F_4 \rightarrow {}^3H_6$ transition in the wavelength range 1600 nm $< \lambda <$ 1950 nm. The measurement was done with a resolution bandwidth of 2 nm. Ti:Tm:$LiNbO_3$ waveguide laser lines reported by Madrid [17] and Southampton [16] are also shown.

dicated in the figure. As the measurement was done by collecting light from behind the waveguide, the actual shape of the fluorecence spectrum may not be reflected in the measured curve. This is because of potential distortions due to (i) stimulated emission (might result in amplification of the peaks) and (ii) reabsorption (might attennuate some part of the spectrum).

2.3.6 *Transition Cross Sections*

Transition (more specifically, absorption and emission) cross sections quantify the ability of a mterial to absorb/ emit light [31]. In order to perform modeling of waveguide amplifiers (and lasers), we need to know absorption and emission cross sections in addition to Tm doping profile, pump and signal mode distributions and energy level life times. Absorption cross sections of the Tm doped waveguide were calculated from the absorption spectrum as follows:

$$\sigma_a(\lambda) = \frac{\alpha(\lambda)}{N_d(\lambda)} \tag{2.2}$$

where $\sigma_a(\lambda)$ is the absorption cross section at the wavelength λ, α is the corresponding absorption coefficient and $N_d(\lambda)$ is the effective Tm density inside the fundamental mode at the wavelength λ. The absorption coefficients were deduced from the absorption spectrum and the effective Tm density was calculated numerically from the waveguide mode intensity profile and the Tm depth profile. Hence absorption cross sections were calculated using equation 2.2. These are shown in Fig.2.10.

The McCumber relation between emission cross section σ_e and absorption cross section σ_a is

$$\sigma_e(\nu) = \sigma_a(\nu) e^{\frac{\epsilon - h\nu}{kT}} \tag{2.3}$$

where, $\sigma_e(\nu)$ is the emission cross section at the optical frequency $\nu(= \frac{c}{\lambda})$, $\sigma_a(\nu)$ is the absorption cross section, k is Boltzmann's constant, h is Planck's constant, ϵ is the net free energy to excite one Tm ion from the $^3H_6$ level to the $^3F_4$ level at temperature T. The net free energy was determined as described by Cantelar [30] assuming that the Tm energy level distribution in both cases are the same. This is justified by the fact that the absorption cross section spectrum was found to have a good agreement with that reported by Cantelar [30].

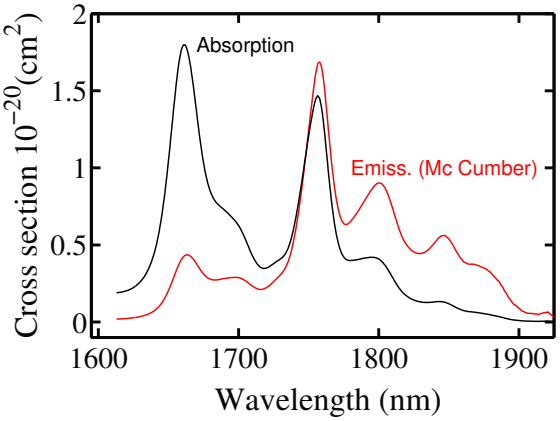

Figure 2.10: TE polarized emission cross sections calculated from absorption cross sections of Ti:Tm:$LiNbO_3$ doped waveguide.

Using equation 2.3 the emission cross sections from the corresponding absorption cross sections can be calculated. The cross sections thus obtained (at room temperature) are given in Fig. 2.10. One of the assumptions of the McCumber theory is that the Stark splitting of the higher excited state ($^3H_4$ level, in this case) is of the order of k_BT ($\sim$ 200 cm^{-1}). In the case of Tm:LN, according to the energy level structure given by Cantelar [30], the splitting of the $^3H_4$ level is 410.4 cm^{-1}. In cases where the Stark splitting is larger than k_BT, the McCumber theory over estimates the lower energy part of the spectrum [32]. Such effects are already reported in RE doped glasses [33].

2.4 CONCLUSIONS

In the first part of this chapter the fabrication of Ti:Tm:Li:NbO_3 waveguides by diffusion doping method is briefly described. The characterization of the waveguides fabricated by means of scattering loss and near field measurements are subsequently discussed. The studies on

properties of the waveguide due to Tm doping (absorption and fluorescence) are also presented. The transition cross sections of the Tm-doped waveguide which are important from the point of view of amplifier/laser fabrication using the waveguide are also determined for the first time via the McCumber theory. Emission cross sections can be determined by measuring the fluorescence spectrum of emission perpendicular (so that effects of re-absorption and amplification can be minimized) to the waveguide. Such a measurement would allow a cross check of the emission cross sections determined by McCumber theory.

3

Ti:Tm:$LiNbO_3$ WAVEGUIDE AMPLIFIER

3.1 INTRODUCTION

From the transition cross section spectra (Fig. 2.10) determined from absorption measurements, it is clear that optical amplification is possible with a pumped Ti:Tm:$LiNbO_3$ waveguide for signal wavelengths beyond 1750 nm. This is because in this spectral region the emission cross section is larger in comparison to the absorption cross section for a given wavelength. Small signal gain measurements were done with the 15 mm long Ti:Tm:$LiNbO_3$ waveguide. The results, which are presented in this chapter, demonstrate that broad-band optical gain in the wavelength range 1750 nm $< \lambda_s <$ 1900 nm can be achieved using a Ti:Tm:$LiNbO_3$ waveguide as an amplifier.

3.2 IN-BAND PUMPING SCHEME

3.2.1 *General Considerations*

One of the preconditions to achieve optical amplification by making use of stimulated emission is the creation of population inversion (i.e., for the case of Ti:Tm:$LiNbO_3$, the number of Tm atoms in excited state should be larger than in the ground state) in the gain medium [34]. One possibility to create a population inversion in the Ti:Tm:$LiNbO_3$ waveguide is by making use of an absorption band of the gain medium (optical pumping). The most prominent absorption band of Tm is centered at 795 nm. The corresponding atomic transitions are shown in Fig. 2.6(left). By using 795 nm laser light Tm atoms can be excited to the $^3F_4$ level, creating a population inversion between the the $^3H_6$ (ground) and the $^3F_4$ (laser) levels. Optical pumping by laser light at 795 nm is the widely used approach in realizing Tm lasers. Some examples can be found in [18, 19, 16, 29]. The choice of the 795 nm pump wavelength is due to the strong absorption[1] at this wavelength. One of the interesting feature of this pumping scheme is the Tm-Tm cross relaxation process, which results in the excitation of two Tm atoms at the expense of a pump photon. Relatively large Tm concentration is needed to take advantage of this process in the case of Tm:$LiNbO_3$ [29]. Indiffusion of Tm to achieve the required Tm concentration would result in increased

1 predominantly TE polarised in the case of Ti:Tm:$LiNbO_3$ and ~ 3 times larger in comparison to that at 1660 nm [30].; see Fig. A.3 for the corresponding absorption spectrum of a Ti:Tm:$LiNbO_3$ waveguide fabricated at Paderborn.

surface roughness (as noted by our study in this direction; see Fig. 3.1) and consequently larger waveguide scattering losses.

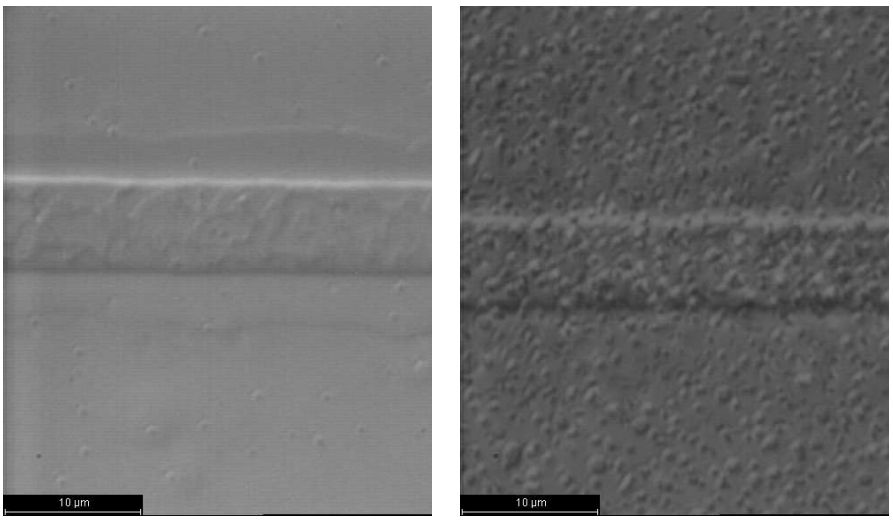

Figure 3.1: Micrographs of waveguides (view from top) from sample Pb304z (left; 32 nm thick Tm layer indiffused for 150 hours) and Pb227z (right; 50 nm thick Tm layer indiffused for 150 hours). The increased surface roughness due to thicker Tm layer is visible.

An alternative pumping approach is the so called in-band pumping scheme, where the Tm atoms in the ground state manifold are pumped directly to the manifold which includes the laser level (instead of having an intermediate level as in the case of pumping Tm atoms using 795 nm light). A recent example of an in-band pumped Tm laser can be found in [35]. The measured absorption spectra (Fig. 2.8) show two strong absorption bands centered around 1660 nm and 1758 nm for TE polarised light. The corresponding absorption is not so strong for TM polarised light. For in-band pumping, the strong Tm absorption bands around 1660 nm or 1758 nm can be exploited. The corresponding transitions are shown in Fig.2.6 (right). The best choice of pump wavelength would be 1660 nm, as will be shown later. The Ti:Tm:$LiNbO_3$ waveguide amplifer and laser(s) mentioned in this thesis are in-band pumped at 1650 nm. The choice of the pump wavelength was mainly due to the availability of a commercial laser diode operating at that wavelength. Pumping at 1660 nm would excite Tm atoms from the lower lying multiplets of $^3H_6$ level to the higher lying multiplets of $^3F_4$ level and subsequently they relax very fast (relaxation time ~ 1 ps) to the lower lying levels of $^3F_4$ multiplet due to thermalisation. As the overall population of both multiplets follows the Boltzmann distribution, a population inversion between the lower levels of $^3F_4$ multiplet and higher lying levels of $^3H_6$ multiplet can be achieved by relatively low pump powers. In this case the gain medium (Tm:$LiNbO_3$) acts as a four level system. On the other hand, short wavelength transitions (1762 nm, as an example)

correspond to a three level system. In that case population inversion can be achieved only with a relatively higher pump rate. As the in-band pumping scheme does not rely on cross relaxation processes (as in the case of pumping at 795 nm) to achieve population inversion, optical amplification can be achieved with moderate Tm concentrations. In-band pumping scheme is already demonstrated in the case of Ti:Er:$LiNbO_3$ waveguide amplifiers [36] by exploiting the strong absorption of Er:LN at 1480 nm.

The attempts to make use of the $^3H_6 \rightarrow {}^3H_4$ transition (795 nm) for pumping did not yield any promising results and this outcome was a strong motivation to consider other pumping schemes. The reasons for the failure are thought to be due to (i) photorefraction occuring in lithium niobate at short wavelengths, (ii) poor overlap between the fundamental waveguide mode at 795 nm and laser (signal) mode and (iii) poor overlap between the higher order waveguide mode(s) at 795 nm which also would be excited (usually) and laser (signal) mode. The effect of photorefraction is strongly reduced at longer wavelengths and hence the in-band pumping scheme does not suffer from detrimental effects due to photorefraction. A third reason which favors the in-band pumping scheme is the fact that the overlap of pump mode with the signal mode is much better compared with the fundamental mode at 795 nm. This reduces the attenuation of signal mode due to absorption at unpumped regions of the waveguide which improves the pumping efficiency.

3.2.2 *Choice of Pump Wavelength*

Theoretical modeling of Ti:Tm:$LiNbO_3$ waveguide amplifiers and laser presented in this thesis was done by the software R P Fiber Power (RPFP) [37]. The theoretical model implemented by RPFP is described briefly in section 3.3. Here modeling results concerning the choice of pump wavelength for the case of an in-band pumped 15 mm long Ti:Tm:$LiNbO_3$ waveguide amplifier are presented.

Three wavelengths from the 1660 nm absorption band (1642 nm, 1660 nm and 1674 nm) and 1758 nm were chosen as the pump wavelengths. A coupled pump power of 13.5 mW was assumed. The outcome of this set of calculations is shown in Fig. 3.2. Net gain corresponds to the calculated gain including the waveguide scattering losses. From the calculated results, it is clear that 1660 nm is the best pump wavelength for in-band pumping of a 15 mm long Ti:Tm:$LiNbO_3$ waveguide amplifier, as at that pump wavelength, maximum gain can be achieved with the same coupled pump power level. On the other hand pumping at 1758 nm is not as efficient (Fig. 3.3). This is due to the the fact that at 1758 nm the difference between absorption and emission cross sections is the smallest among all the pump wavelengths considered. Consequently some of the excited Tm atoms con-

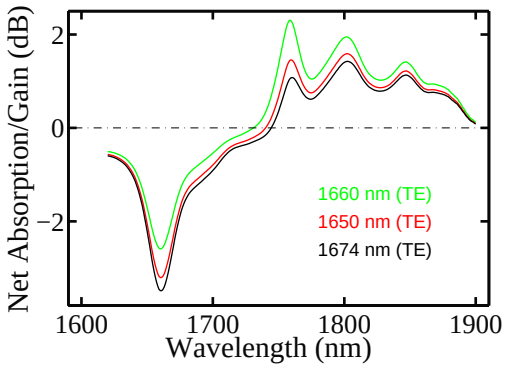

Figure 3.2: Calculated net absorption/gain spectra of a 15 mm long Ti:Tm:$LiNbO_3$ waveguide amplifier, single pass pumped at 1642 nm, 1660 nm and 1674 nm (signal and pump are TE polarized) with a coupled pump power of 13.5 mW.

tribute back to the amplification of pump and this makes this pumping scheme less efficient. The attempts to procure a 1660 nm diode laser were not fruitful and hence it was decided to use a Fabry-Pérot diode laser operating at 1650 nm for pumping the amplifier (and laser cavities) mentioned in this thesis, as such a diode laser could readily be obtained.

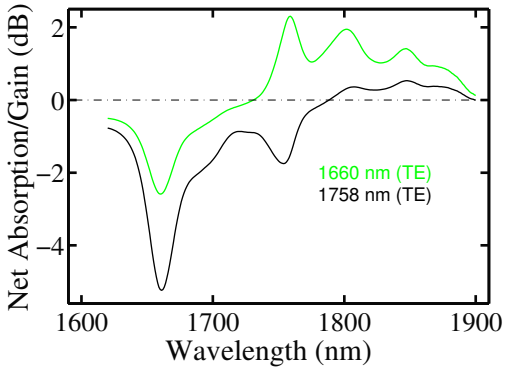

Figure 3.3: Calculated net absorption/gain spectra of a 15 mm long Ti:Tm:$LiNbO_3$ waveguide amplifier, single pass pumped at 1650 nm and 1758 nm (signal and pump are TE polarised) with a coupled pump power of 13.5 mW.

3.3 MODELING

Theoretical modeling of waveguide amplifier and laser presented in this thesis were done with the commercial software RP Fiber Power [37]. The physical model implemented by the software assumes the following [38]: *(i.)* The doping profile is constant in longitudinal direc-

tion, *(ii.)* the gain medium is homogeneously broadened, *(iii.)* spatial hole burning is neglected *(iv.)* the intensity distribution of an optical channel is preserved at all times *(v.)* there is no coherence between different optical channels *(vi.)* there are no nonlinear effects (stimulated Raman and Brillouin scattering) arising in the laser or amplifier and *(vii.)* the population distributions within each Stark level manifold of laser active ions are in thermal equillibrium.

Consider the two atomic energy levels E_1 and E_2 of a laser active medium shown in Fig. 3.4. There can be three processes shown in the figure between these two energy levels which involves a photon. In the case of absorption, an incoming photon (having an energy equivalent to the difference of energies of the two levels, $h\nu = E_2 - E_1$) gets absorbed by the atom resulting in the atom getting excited to the higher level. When an incoming photon of energy $h\nu$ interacts with an excited atom, the atom can relax to the lower energy level emitting a second photon. This process is called stimulated emission. The third process, called as spontaneous emission occurs when the excited atom relaxes to the lower energy level by emitting a photon of energy $h\nu$. In the case of stimulated emission the resulting pho-

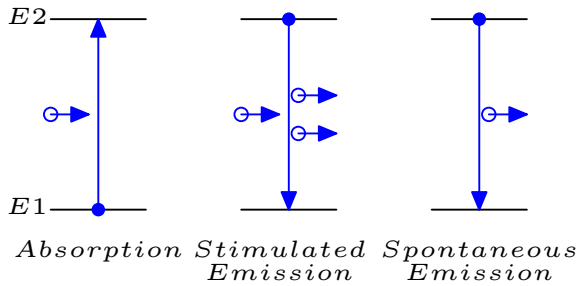

Figure 3.4: Depiction of absorption, stimulated emission and spontaneous emission processes in a laser active medium.

ton has the same quantum mechanical properties as the stimulating photon. An amplifier (and a laser) relies on stimulated emission for its operation. On the other hand spontaneous emission (and the corresponding stimulated emision arising from spontaneous emission which results in amplified spontaneous emission or ASE) is a source of noise in an optical amplifier (and laser) which relies on stimulated emission for its operation.

For the case of an optical waveguide doped with laser active ions having an energy level scheme as shown in Fig. 3.4 at position z (longitudinal direction), the local gain coefficient g is given by,

$$g(z,\lambda) = N_{RE}[n_2(z)\sigma_{21}(\lambda) - n_1(z)\sigma_{12}(\lambda)] \tag{3.1}$$

where N_{RE} is the density of the laser active atoms, $n_2(z)$ is the fraction of laser active atoms in level 2, $n_1(z)$ is the fraction of laser active atoms in level 1, $\sigma_{21}(\lambda)$ is the emission cross section at wavelength λ

and $\sigma_{12}(\lambda)$ is the absorption cross section, z is the longitudinal position in the waveguide. Equation 3.1 is valid for an infinitesimal length of the waveguide, where $n_2(z)$ (and consequently $n_1(z)$) remains a constant. For a waveguide length L, the total amplification is given by

$$G(\lambda) = exp\left(\int_0^L g(z,\lambda)dz\right) \tag{3.2}$$

Taking transverse dimensions into account, the gain has contributions from different positions and is given by

$$g(z,\lambda) = \int_{-\infty}^{\infty}\int_{0}^{-\infty} N_{RE}(y)[n_2(x,y,z)\sigma_{21}(\lambda) - n_1(x,y,z)\sigma_{12}(\lambda)]\psi(x,y,z)dxdy \tag{3.3}$$

where $\psi(x,y,z)$ is the intensity distribution of the waveguide signal (or pump) mode being considered. In the numerical model implemented by R P Fiber Power, the waveguide is sliced in x and y directions (lateral dimensions). The contribution to gain (or absorption) at different z locations from each cube of volume $dxdydz$ is numerically added and in this way the amplification by a given length of waveguide for a given absorbed pump power can be calculated, if the wavelength dependent transition cross sections, RE doping profile and waveguide mode intensity profiles for pump and signal are known. All theoretical calculations of Tm:Ti:$LiNbO_3$ waveguide amplifier and laser presented in this dissertation have been done with emission cross sections determined from McCumber theory.

3.3.1 *Gain Spectra*

In this section the calculated gain spectra of two waveguide amplifiers (l = 90 mm (Fig. 3.5) and 15 mm (Fig. 3.7)) at three different coupled pump powers (25 mW, 50 mW and 100 mW) are presented. The pump wavelength is 1650 nm (TE polarized). Calculations were performed with input signal power kept at 1 µW and α_s= 0.1 dB/cm.

The potential for broadband optical gain for signal wavelengths from 1750 nm $< \lambda_s <$ 1900 nm is evident from the calculated gain curves for a coupled pump power of 100 mW. As the waveguide length is increased the ground state absorption also increases as expected. This is evident from the 'gain' (or absorption) spectra corresponding to the unpumped case of the two amplifier lengths. In the case of a longitudinally (single pass[2]) pumped waveguide, the

2 residual pump beam from the waveguide end is not reflected back to the waveguide.

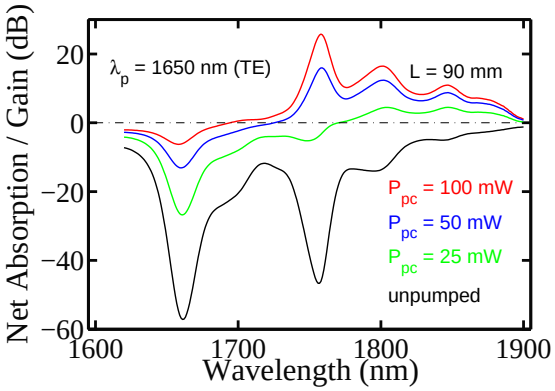

Figure 3.5: Calculated net absorption/gain spectra of a 90 mm long waveguide amplifier at three different coupled pump powers (signal and pump are TE polarised).

typical distribution of pump power is shown in Fig. 3.6. From the pumped end of the waveguide, the pump power gradually becomes smaller and smaller depending on the strength of pump absorption. The pump power required to keep a length of waveguide pumped (i.e., Tm atoms of gain media are maintained in the excited state) becomes larger and larger as the waveguide length is increased. The distribution of pump power for the case of a 90 mm long waveguide for three different coupled pump powers are shown in Fig. 3.6. With

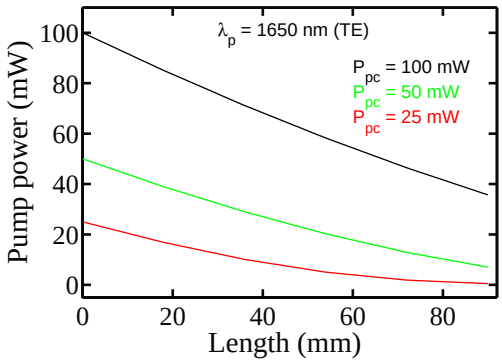

Figure 3.6: Distribution of pump power across a 90 mm long waveguide amplifier at three different coupled pump powers.

25 mW of coupled pump power, the length of the waveguide which is pumped is 8 cm. In other words, the coupled pump power (25 mW in this case) is absorbed completely by a 8 cm long waveguide section. Beyond 8 cm, the waveguide is not pumped and consequently that section of the waveguide absorbs signal radiation ($\lambda_s > 1750$ nm). With 50 mW of coupled pump power, the situation is improved. A 90 mm long waveguide is pumped throughout its length in this case (14% pump transmission). With 100 mW coupled pump power, the

situation is improved even further. This is because of the fact that the rate of pumping of Tm atoms (in an infinitesimal section of the waveguide) is directly proportional to the incident pump power.

With pumping, Tm atoms in the ground state are excited and consequently the absorption coefficient (at pump wavelength and signal wavelengths) becomes smaller and smaller as the pump power is increased. This is because of the fact that the population in the ground state becomes smaller and smaller as pump power is increased gradually. Absorption at any given wavelength will be bleached (i.e., absoption coefficient becomes zero) when the atomic population of the two sublevels (of the two manifolds) involved in contributing to the emission (or absorption) of a given wavelength become equal. When there is inversion between the two sublevels contributing to the emission of a given wavelength (i.e., when the pump power is larger than what is required to bleach the absorption), it is possible to amplify the signal power corresponding to that wavelength. Whether a given signal wavelength will be amplified or not, depends on the overall gain (and absorption) experienced by the signal beam as it passes through the amplifier. This becomes clear from the calculated gain curve for 25 mW of coupled pump power in the case of a 90 mm long waveguide. As said above, there is a 1 cm long section of the waveguide which is unpumped and consequently signal radiation (at all wavelengths) will be absorbed by this section. However from the gain spectra it is evident that a positive net gain is possible at signal wavelengths larger than 1775 nm. This is because of the fact that the gain experienced by these signal wavelengths while passing through the pumped section is larger in comparison to the loss from the unpumped section. On the other hand the gain experienced by shorter wavelengths while traversing through the pumped section is not sufficient to overcome the absorption. Consequently they are attennuated instead of being amplified. But at higher coupled pump powers (50 mW, for example) the gain experienced by the whole of the signal spectrum (1750 nm $< \lambda_s <$ 1900 nm) becomes positive.

As the absorption at longer wavelengths is relatively weaker (in the unpumped case) bleaching of absorption at these wavelengths occurs with relatively low coupled pump powers because the required population of the higher lying sublevel can be realized at low pump powers. The underlying reason for this is the Boltzmann distribution of energy levels in the ground and excited state multiplets. By the same reasoning it is clear that positive net gain is achieved first at long wavelengths as the pump power is gradually increased. The pump power required to achieve (bleaching and subsequently) net gain at shorter wavelengths (below 1770 nm) is relatively larger in comparison to that at longer wavelengths (for a given length of the waveguide). This is a consequence of the stronger absorption at short wavelengths in comparison to the longer wavelengths. However as

the number of atoms in the energy levels contributing to the emission at shorter wavelengths is relatively larger in comparison to those contributing to the emission at longer wavelengths when population inversion is achieved throughout the length of the waveguide, the net gain achievable from a given waveguide length is always larger at short wavelengths. This can be seen by comparing the gain spectra for the two different amplifier lengths. As an example for 100 mW

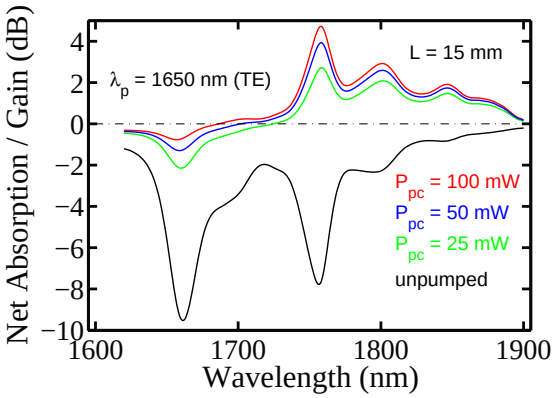

Figure 3.7: Calculated net absorption/gain spectra of a 15 mm long waveguide amplifier at three different coupled pump powers (signal and pump are TE polarised).

coupled pump power the net gain at 1758 nm achievable from the 90 mm long amplifier is 25.7 dB and that from the 15 mm long amplifier is 4.7 dB. For the same coupled pump power level, the gain at longer wavelengths are smaller than these values.

With the diffusion technology developed in our lab, so far we have fabricated waveguide samples up to 9 cm in length. One of the best waveguides developed so far (α_s= 0.03 dB/cm, waveguide length = 9 cm) was used in the fabrication of a Ti:Er:$LiNbO_3$ waveguide laser similar to that described in [14]. Due to its low scattering loss value, the laser wavelength was 1614 nm, the longest emission wavelength which was observed so far from a Fabry-Pérot type Ti:Er:$LiNbO_3$ waveguide laser (see Fig. B.1). In the same way it should be possible to make Tm doped waveguides of good quality with lengths up to 10 cm [3]. In what follows the calculated results corresponding to the net gain achieveable from different amplifier (Ti:Tm:$LiNbO_3$ waveguide) lengths up to 10 cm at different coupled pump powers at four different signal wavelengths are given. The four signal wavelengths chosen were 1758 nm, 1800 nm , 1858 nm (three emission peaks; see fluorescence spectrum Fig. 2.9) and 1890 nm (laser wavelength; see section 4.5.1). Calculations were performed with input signal power kept at 1 µW and α_s= 0.1 dB/cm.

3 LN wafers with a diameter of 4 inches are currently commercially available.

Fig. 3.8 shows the calculated single pass gain at 1758 nm as a function of waveguide lengths for four different coupled pump powers

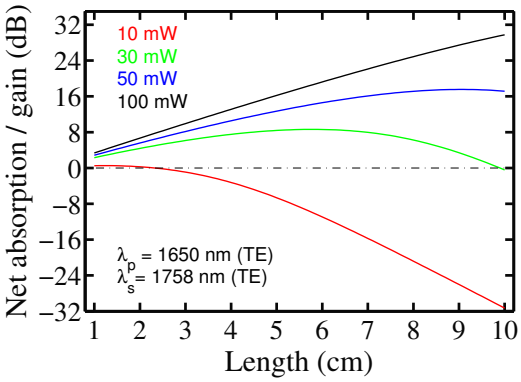

Figure 3.8: Calculated gain at 1758 nm (TE polarization) as a function of waveguide length for four different coupled pump powers.

10 mW, 30 mW, 50 mW and 100 mW at 1650 nm. The coupled pump power needed to just bleach the absorption (and achieve amplification) becomes larger and larger as the waveguide length is increased. At this wavelength with 10 mW of coupled pump power a waveguide length of 2.3 cm can be maintained at bleaching level (i.e., absorption coefficient at 1758 nm is zero). With 30 mW of coupled pump power the waveguide length which can be maintained at bleaching level becomes 96 mm. This is a consequence of the three level nature of the gain medium at this wavelength. When the coupled pump power is increased further, the net gain starts to become larger. The calculation result show that with 100 mW of coupled pump power it is possible to achieve a net single pass gain of 30 dB using a 10 cm long waveguide.

Fig. 3.9 shows the calculated gain at 1800 nm as a function of waveguide lengths for different coupled pump powers. The length

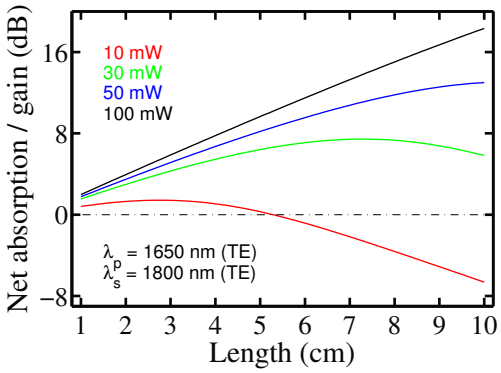

Figure 3.9: Calculated gain at 1800 nm (TE polarization) as a function of waveguide length for four different coupled pump powers.

of waveguide which can be kept at bleaching level with 10 mW of coupled pump power is 5.2 cm at this wavelength. With a coupled pump power of 30 mW, the absorption is not only bleached but amplification (i.e., positive net gain of 5.8 dB) is possible even with a 10 cm long waveguide. These results point to the less prominent three level nature of the gain medium, at this wavelength. With larger coupled pump powers larger gain is achievable from long waveguide lengths. In this case with a coupled pump power of 100 mW a 10 cm long waveguide can yield a net gain of 18.3 dB.

The calculated gain at 1848 nm as a function of different waveguide lengths for different coupled pump powers at are shown in Fig.

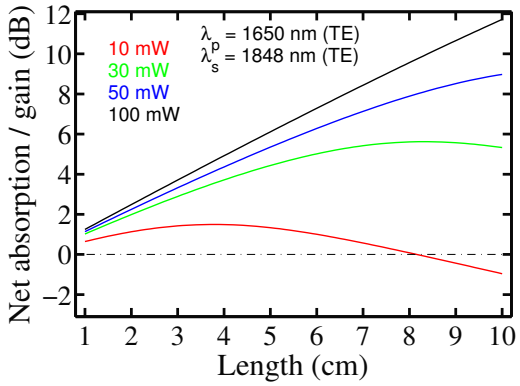

Figure 3.10: Calculated gain at 1848 nm (TE polarization) as a function of waveguide length for four different coupled pump powers.

3.10. The length of the waveguide which can be kept just above the bleaching level at this wavelength is 8.1 cm with a coupled pump power of 10 mW. This is because of the fact that ground state absorption at this wavelength is even smaller than at shorter wavelengths and consequently the inversion necessary to achieve a net gain can be realized at smaller pump powers (than what is required at shorter wavelengths). With 30 mW of coupled pump power a net gain of 5.3 dB can be achieved from a 100 mm long waveguide. At 100 mW coupled pump power with a 10 cm long waveguide, it is possible to achieve a net gain of 11.7 dB at this wavelength.

Fig. 3.11 shows the calculated gain at 1890 nm as a function of waveguide lengths for different coupled pump powers. Modeling results show that the maximum length of waveguide which can be kept above bleacing level with 10 mW of coupled pump power is 7.3 cm. A coupled pump power of 30 mW would yield a gain of 1.5 dB with an amplifier length of 10 cm. With a 10 cm long waveguide and a coupled pump power of 100 mW, a net gain of 3.5 dB can be achieved. The gain values are smaller than the corresponding values calculated for 1848 nm signal wavelength. At this wavelength the gain medium is more closer to a four level gain medium. Hence one would expect

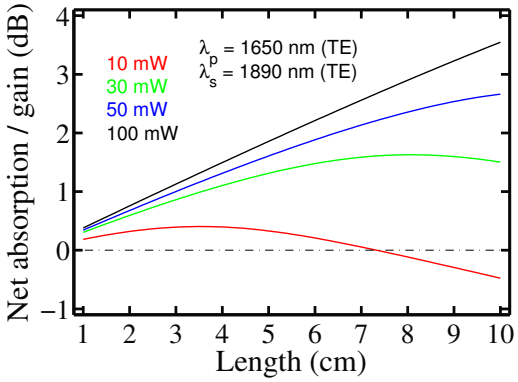

Figure 3.11: Calculated gain at 1890 nm (TE polarization) as a function of waveguide length for four different coupled pump powers.

that an even longer waveguide length than that at 1848 nm signal wavelength could be kept above bleaching level with 10 mW of coupled pump power. But the modeling result does not favor this conclusion. The discrepancy is thought to arise from the inapplicability of McCumber theory in the estimation of emission cross sections at these long wavelengths and/or the inacuracies in the estimation of waveguide propagation losses. Experimental results of small signal gain measurements done with 1.5 cm long amplifier also points this conclusion.

3.3.2 *Power Characteristics*

If the amplifier is pumped harder and harder (i.e., when pump power is increased gradually) the gain of the amplifier at any given wavelength also increases. However this process cannot go on infinitely. This is because, at some point the rate of depletion of the excited atoms will be faster than the rate of pumping (or replenishment of the number of excited atoms). When this happens, the gain of the amplifier becomes saturated. This is shown in Figs. 3.12 and 3.13. Fig. 3.12 shows the variation of gain of two amplifier lengths 30 mm and 90 mm at $\lambda_s = 1758$ nm as a function of the coupled pump power. At low pump powers the gain increases exponentially. But as the pump power is increased further the gain of the amplifiers starts to get saturated. The saturated gain of the 30 mm amplifier at 30 dBm coupled pump power is 12 dB where as that for the 90 mm long amplifier is 36 dB. In this case, the saturated gain scales proportional to the length. The situation is the same at a different signal wavelength $\lambda_s = 1850$ nm. Fig. 3.12 shows the variation of gain of two amplifier lengths 30 mm and 90 mm at $\lambda_s = 1758$ nm. At 30 dBm coupled pump power, the 30 mm long amplifier yields a gain of 4 dB whereas the 90 mm long waveguide yields 12 dB.

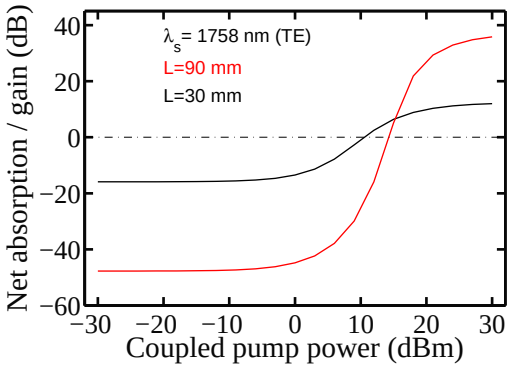

Figure 3.12: Calculated net absorption/gain of 30 mm and 90 mm long Ti:Tm:$LiNbO_3$ waveguide amplifiers as a function of coupled pump power for signal wavelength λ_s = 1758 nm (signal and pump are TE polarised).

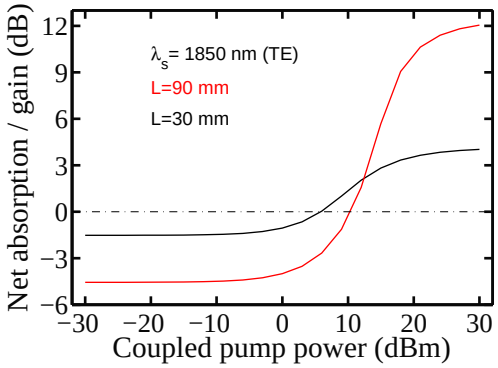

Figure 3.13: Calculated net absorption/gain of 30 mm and 90 mm long Ti:Tm:$LiNbO_3$ waveguide amplifiers as a function of coupled pump power for signal wavelength λ_s = 1850 nm (signal and pump are TE polarised).

3.3.3 *Double Pass Pumping*

The modeling results presented so far considered single pass pumped amplifiers. The calculated internal distribution of pump power as a function of position inside waveguide for a 15 mm long waveguide amplifier is shown in Fig. 3.14. The residual pump power at the end of a 1.5 cm long amplifier is 8.4 mW. It is possible to make better use of this residual pump power by reflecting it back into the cavity by placing a pump reflector mirror at the end of the waveguide. The calculated result for a 1.5 cm long amplifier with an ideal pump reflector (pump reflection = 100%) is also shown in Fig. 3.14. The pump power distribution is at a higher level than with the case of single pass pumping. This would mean that the pumping rate along the waveguide is better than with the single pass pumping scheme

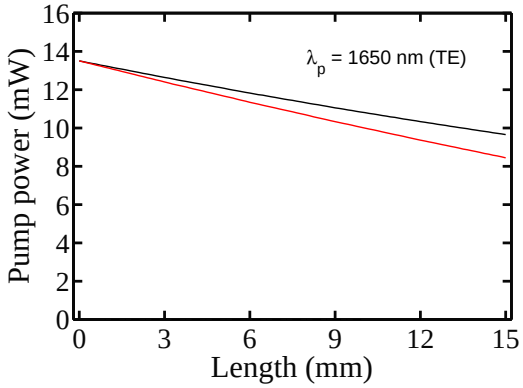

Figure 3.14: Calculated internal distribution of pump power as a function of position inside waveguide for a 15 mm long waveguide for 13.5 mW coupled pump power for single pass (red) and double pass (black) pumping schemes.

and consequently we can achieve an even higher gain where the signal is still single pass. Fig. 3.15 shows the comparison between both single and double pass pumped amplifiers. For simulations, the ideal back side mirror (pump reflectivity = 100% and signal reflectivity = 0%) is considered. The double pass pumping scheme results in an

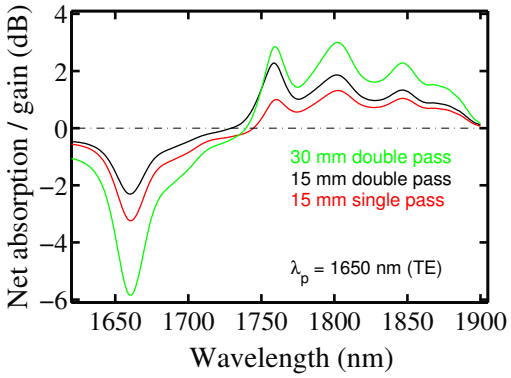

Figure 3.15: Calculated net absorption/gain spectra of a 15 mm long and 30 mm long Ti:Tm:$LiNbO_3$ waveguide amplifier for single and double pass pumping at 1650 nm (signal and pump TE polarized) for 13.5 mW coupled pump power.

improved gain spectrum which is shown in black (in comparison to the single pass pumped case shown in red) in the figure. An increase in the waveguide length by a factor of 2 together with double pass pumping improves the situation even further as shown by the green curve in Fig. 3.15.

Additional gain spectra for a 30 mm long waveguide with double pass pumping scheme were calculated and the results are shown in Fig.3.16. With just few milliwatts of coupled pump power (specifically

with 4 mW), it is possible to achieve a net gain in the long wavelength side. This shows the potential for a Fabry-Pérot type laser fabricated with such a waveguide amplifier to operate in the long wavelength side of the emission spectrum of Ti:Tm:$LiNbO_3$. Such a

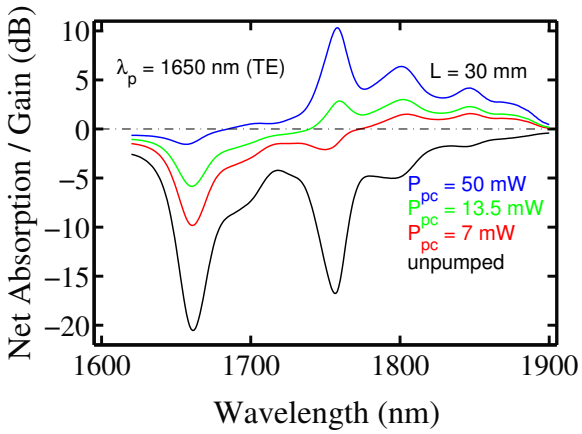

Figure 3.16: Calculated net absorption/gain spectra for a double pass pumped 30 mm long Tm doped waveguide. Both pump and signal are TE polarised.

laser is demonstrated in chapter 4.

3.3.4 *Further Comments*

The modeling results presented above did not take ASE into account. Although, amplification of spontaneous emission is a stimulated process, the energy of the excited atoms is not used in the amplification of the input signal (or laser signal in the case of a laser), but is in a way 'lost' and consequently it is a parasitic process. As a result when ASE is also included in the calculation, the corresponding net gain values will be lower than the case when ASE is not taken into account. ASE becomes significant in the case where the gain of the amplifier is large ($<$ 20 dB) [39] because then it can deplete the inversion thus reducing the gain of the amplifier.

3.4 EXPERIMENTAL INVESTIGATIONS

3.4.1 *Experimental Setup*

The schematic of the experimental setup which was developed to investigate the Ti:Tm:$LiNbO_3$ waveguide amplifier is shown in Fig. 3.17. A fibre coupled Fabry-Pérot type diode laser with a peak wavelength of 1650 nm was used as pump laser. Its output fibre was spliced to a fibre optical polarization controller and a fibre optical isolator in series. To measure optical absorption and gain spectra, unpolarized chopped

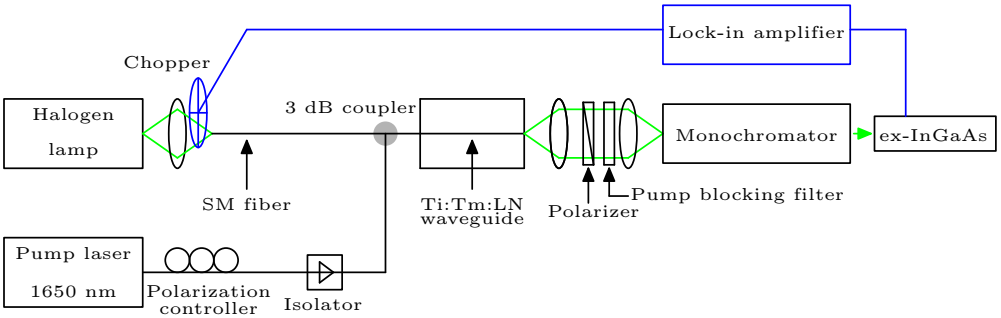

Figure 3.17: Schematic of the experimental setup which was used to investigate the Ti:Tm:$LiNbO_3$ waveguide amplifier.

light (signal; infront of 3 dB coupler power when measured with 2 nm resolution bandwidth at 1600 nm, the power density was ~ 400 pW) from a halogen lamp was superimposed to the pump radiation by a fibre optical 3 dB coupler and then butt coupled into the 15 mm long Tm-doped waveguide. The output was imaged to the input of a monochromator (resolution bandwidth set to 2 nm; independently measured with 1600 nm emission from an extended cavity laser). A polarizer (specified extinction ratio of 60 dB) in the free space beam path determined the polarization of the signal to be measured; a special wavelength filter blocked to a large extent the transmitted pump radiation (attenuation ~ 18 dB). A thermo-electrically cooled ("wavelength extended") InGaAs photodiode was used to measure with a lock-in technique the (spectrally resolved) transmitted signal. The measurements were controlled by a computer which also recorded the data. To determine a gain spectrum at a given pump power level, two measurements were performed, one with pumping (TE polarized in all cases) and the second without pumping. By dividing the measured data from the pumped case with those obtained without pumping, the corresponding gain spectrum was obtained. The gain spectrum thus determined do not include scattering losses.

3.4.2 *Experimental Results*

Fig. 3.18 shows (as open circles) the measured gain spectra for three different pump powers. At shorter wavelengths close to the pump wavelength, gain measurements could not be made as the noise levels were high enough to saturate the detection circuit. At those wavelengths, the pump blocking filter was not sufficient to attenuate the transmitted pump power completely.

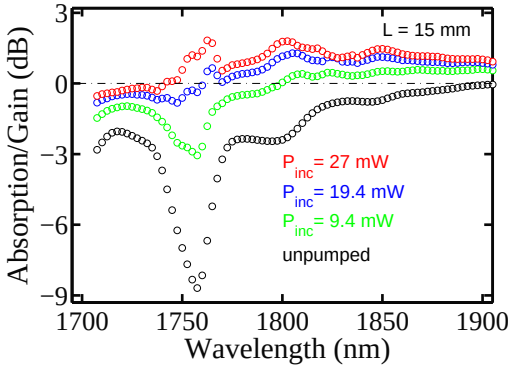

Figure 3.18: Measured gain spectra of a 15 mm long Tm:Ti:$LiNbO_3$ waveguide amplifier, pumped at 1650 nm (signal and pump TE polarized). Parameter is the incident pump power P_{inc} (λ_p = 1650 nm).

3.5 DISCUSSION

3.5.1 *Comparison of Experimental and Modeling Results*

As the next step, the agreement between measured and calculated gain spectra was checked. Along with the cross section data (absorption cross sections and McCumber emission cross sections), calculated TE mode intensity profiles, upper state life time of 2.4 ms [29] and waveguide propagation loss of 0.1 dB/cm for pump and signal beams were given as the inputs for performing calculations. The signal input power used for the calculations is 1 µW (small signal amplification). Waveguide mode intensity profiles were calculated by Focus, a software developed by Strake [25].

The outcome of modelling is shown in Fig. 3.19 (as lines). As this set of measurements were done one after the other the pump coupling efficiency was assumed to be the same in all cases. During the experiments, the transmitted signal power level behind the waveguide was checked before (and after) all measurements and in this way the consistency of input coupling and over all stability of the experimental setup was confirmed. The modeling was done by varying the coupled pump power in order to find out the best choice which fits with the measurement result (judgement by eye). From Fig. 3.19, we see that there is a reasonably good agreement between measured and calculated data sets for a pump coupling efficiency of 50%. In general, the agreement of modeling and experimental results is very good, demonstrating the reliability of the theoretical model used; this good agreement is also a consequence of the experimentally determined input parameters for the calculations. Remarkable is, that optical gain surpasses the zero dB level in the whole wavelength range 1750 nm $< \lambda <$ 1900 nm with a coupled pump power of 13.5 mW only, indicat-

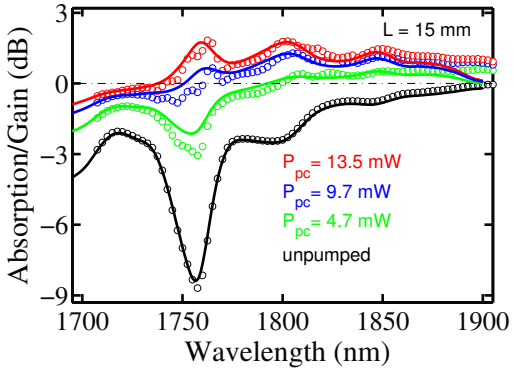

Figure 3.19: Calculated net absorption/gain spectra (lines) of a 15 mm long Tm:Ti:$LiNbO_3$ waveguide amplifier, pumped at 1650 nm (signal and pump TE polarized), compared with experimental results (open circles). Parameter is the coupled pump power P_{pc} (λ_p = 1650 nm).

ing the potential for tunable waveguide lasers in that range. The main gain peaks, already known from the fluorescence data (Fig. 2.9), arise at somewhat higher pump power levels. However, at the long wavelength side ($\lambda >$ ~1880 nm), the agreement of theory and experiment becomes poor. This could be attributed to the limited applicability of the McCumber theory in this wavelength range.

Results of small signal gain measurements presented above, demonstrate that broadband amplification in the spectral range 1750 nm $<$ $\lambda <$ 1900 nm using a 15 mm long Ti:Tm:$LiNbO_3$ waveguide amplifier is possible. In the remaining part of this section, additional modeling results, together with experimental results of the measurements performed with the 15 mm long waveguide amplifier are presented. The four signal wavelengths chosen were 1758 nm, 1800 nm , 1858 nm (three emission peaks; see fluorescence spectrum) and 1890 nm (laser wavelength; see section 4.5.1).

Fig. 3.20 shows the calculated net gain curve and measured net gain data (i.e. gain including scattering losses of the waveguide) curves at 1758 nm signal wavelength for a waveguide length of 15 mm and single pass pumping. From the measured gain data 0.3 dB was subtracted as scattering loss to obtain the net gain values. At this signal wavelength absorption is bleached with 9 mW of coupled pump power. This is because of the three level nature (and the consequent reabsorption of signal wavelength) of the gain medium at this wavelength range of the fluorescence spectrum of Ti:Tm:$LiNbO_3$. A higher coupled pump power (in comparison with longer signal wavelengths, as will be shown later) is needed to achieve inversion. From Fig. 3.20, it is clear that there is a reasonable agreement between calculated and measured values. With 30 mW coupled pump power, more than

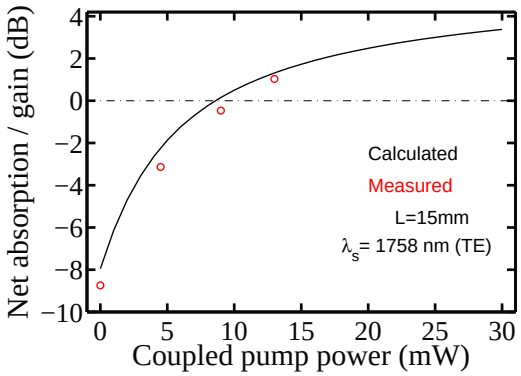

Figure 3.20: Measured (red) and calculated single pass net gain at 1758 nm (TE) for a waveguide length of 15 mm as function of coupled pump power (TE).

3 dB gain at λ_s=1758 nm with single pass pumping scheme could be achieved.

The calculated net gain curve and measured net gain data at 1800 nm signal wavelength are shown in Fig. 3.21. At this signal wave-

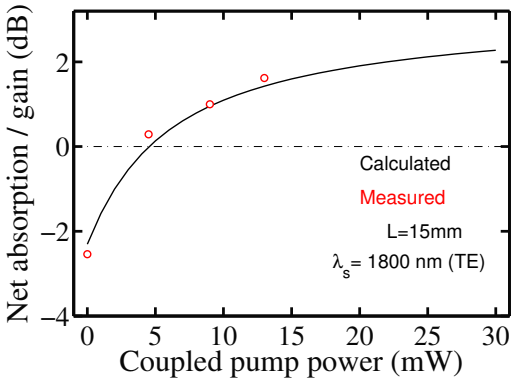

Figure 3.21: Measured (red) and calculated single pass net gain at 1800 nm (TE) for a waveguide length of 15 mm as a function of coupled pump power (TE).

length absorption is bleached with only 5 mW of coupled pump power. The three level nature of the gain medium is less prominent at 1800 nm and consequently signal re-absorption is much lower at this wavelength in comparison to that at 1758 nm. From Fig. 3.21, we see that there is a good agreement between calculated and measured values. In this case with 30 mW coupled pump power, net gain more than 2 dB at λ_s=1800 nm could be achieved.

Fig. 3.22 shows the calculated net gain curve and measured net gain data at 1850 nm signal wavelength. The three level nature of the gain medium is even less prominent (absorption in the unpumped case is only 0.7 dB) than at 1800 nm at this wavelength and consequently

signal re-absorption is much lower. The absorption is bleached with

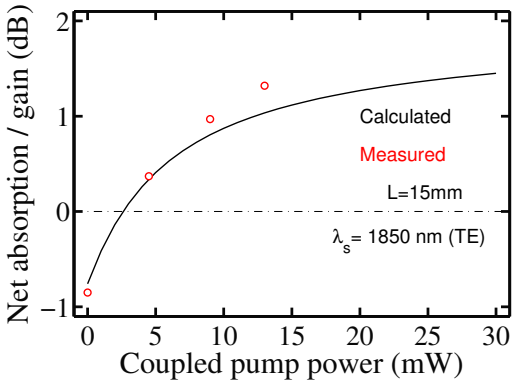

Figure 3.22: Measured (red) and calculated single pass net gain at 1850 nm (TE) for a waveguide length of 15 mm as a function of coupled pump power (TE).

3 mW of coupled pump power in this case. In this case also, there is a reasonable agreement between calculated and measured values. With 30 mW coupled pump power, more than 1.5 dB gain at λ_s=1850 nm could be achieved.

The calculated net gain curve and measured net gain data at 1890 nm signal wavelength are shown in Fig. 3.23. In this case the gain

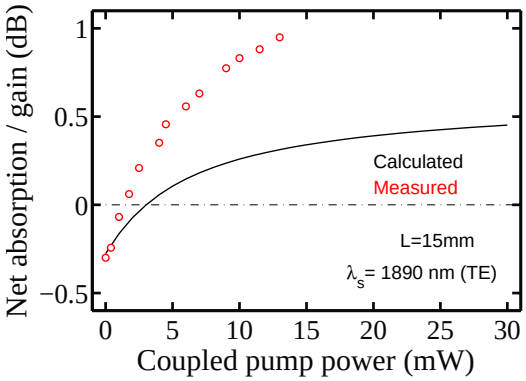

Figure 3.23: Measured (red) and calculated single pass net gain at 1890 nm (TE) for a waveguide length of 15 mm as a function of coupled pump power (TE).

medium is close to an ideal four level system (absorption in the unpumped case is only 0.27 dB) than at 1850 nm and consequently signal re-absorption is practically zero. According to the modeling result, the absorption is bleached with 4 mW of coupled pump power. But from the experimental result bleaching of absorption occurs with just 1.8 mW of coupled pump. From Fig. 3.23, it is clear that the agreement between calculated and measured values becomes poor in com-

parison to the corresponding outcomes at shorter wavelengths. This surprising result is believed to be mainly due to the inapplicability of McCumber theory in the estimation of (emission) cross sections (see section 2.3.6) at these long wavelengths and/or the inacuracies in the estimation of waveguide propagation losses (see section 4.4.1).

3.5.2 *Amplifiers for Laser Applications*

The amplifiers discussed so far operated in the single pass pump regime. It was also shown that the usage of the available pump power can be improved by adopting double pass pumping scheme, where the residual single pass pump is reflected back into the amplifier by a pump reflector at the unpumped end of the amplifier. By adopting the same strategy for signal as well (i.e., signal beam also is reflected back) the achievable net gain from a given amplifier length and pump power can be doubled, provided the amplifier is operated in the small signal gain regime. By having a high reflector mirror for signal at both endfaces of an amplifier, a laser can be realized. In that case the signal is amplified as it traverses the length of the amplifier multiple times. As the net gain crosses the zero level, lasing action sets in there after as the pump power is increased the energy from the pump beam is transfered to the laser beam. In practice there is no signal input (as in the case of an amplifier) into a laser cavity. As the pump power is increased, laser action starts from amplified stimulated emission. With the Ti:Tm:$LiNbO_3$ amplifiers mentioned in this chapter, lasers operating at any wavelengths in the gain bandwidth can be realized. In chapter 4, the realization of a laser with a 30 mm long Ti:Tm:$LiNbO_3$ waveguide amplifier is discussed.

3.5.3 *Conclusions*

The results which are presented in this chapter, demonstrate that broadband optical gain in the wavelength range 1750 nm $< \lambda_s <$ 1900 nm can be achieved using a Ti:Tm:$LiNbO_3$ waveguide as an amplifier. Results of small signal gain measurements are found to be in good agreement with the corresponding modeling results for the case of single pass pumping scheme. Modeling results show the possibility to achieve (wavelength dependent) gain of up to 30 dB from a 10 cm long single pass pumped waveguide. The gain achieveable with a given pump power level can be improved by implementing double pass pumping along with a careful choice of waveguide length. Such double pass pumped amplifiers can be used to realize waveguide lasers operating at any of the wavelengths in the broadband signal spectrum where optical gain can be achieved.

4

Ti:Tm:$LiNbO_3$ WAVEGUIDE LASER

4.1 INTRODUCTION

Modeling results presented in chapter 3 show that it is possible to achieve a positive net gain near 1890 nm from a double pass pumped 30 mm long Ti:Tm:$LiNbO_3$ waveguide. The realization and properties of a waveguide laser operating at 1890 nm and 1850 nm with such an amplifier are discussed in this chapter. The highlight of this chapter is the first demonstration of an in-band pumped Ti:Tm:$LiNbO_3$ waveguide laser (i) emitting at the longest emission wavelength, (ii) with the smallest laser threshold and the highest output power reported from a Tm:$LiNbO_3$ waveguide laser so far.

4.2 LASER CAVITY

The laser cavity was formed by two dielectric multilayer mirrors comprising of alternating layers of TiO_2 and SiO_2, vacuum deposited on the end faces of the 30 mm long Ti:Tm:$LiNbO_3$ waveguide, enabling double pass pumping. The pump coupler mirror has a high reflectivity (HR $>$ 90 %) at wavelengths $>$ 1800 nm, but a high transmission (T $>$ 90 %) at the 1650 nm (pump wavelength). The output coupler mirror has a broadband characteristic of high reflectivity (R>95%) in the spectral range 1640 nm $< \lambda <$ 1900 nm . The measured mirror reflectivity curves of both mirrors are given in Fig. 4.1. The calculated finesse of the cavity thus formed is 32 (scattering losses are assumed to be 0.1 dB/cm, λ_s = 1890 nm).

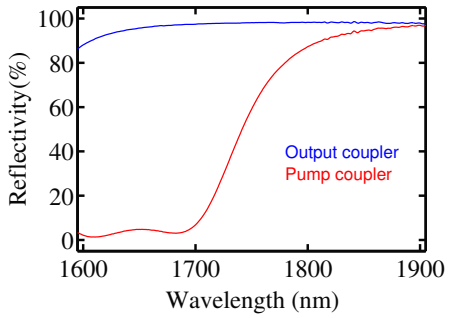

Figure 4.1: Reflectivity of the input mirror (pump coupler;red) and of the output mirror (output coupler;blue) in the wavelength range 1600 nm $< \lambda <$ 1900 nm.

4.3 EXPERIMENTAL SETUP

The experimental set up to investigate the laser is shown in Fig. 4.2. A fiber coupled diode laser with a centre wavelength of 1650 nm was used as pump laser. At the output of the laser a fibre optic isolator (isolation $\geqslant$ 35 dB) and a fibre optic polarization controller were spliced one behind the other to minimize losses. The output fibre of the isolator was kept butt coupled to the end face of the Tm doped waveguide with the pump coupler mirror. Light behind the Tm doped waveguide was collimated by a lens and was coupled into the input port of a 10/90 coupler. The 90% output was sent to a fiber coupled monochromator and the 10% output was used to enable controlled pumping. A thermo-electrically cooled wavelength extended InGaAs photodiode kept behind the monochromator was used to detect the emission of the waveguide laser. Alternatively the 90% beam was send to a photodiode kept connected with an electronic spectrum analyser (or a fast oscilloscope), for performing frequency (or time) domain measurements. The free space beam allowed the measurement of pump and signal polarizations. A pump blocking filter (~18 dB) kept in the free space beam suppressed any residual pump emission.

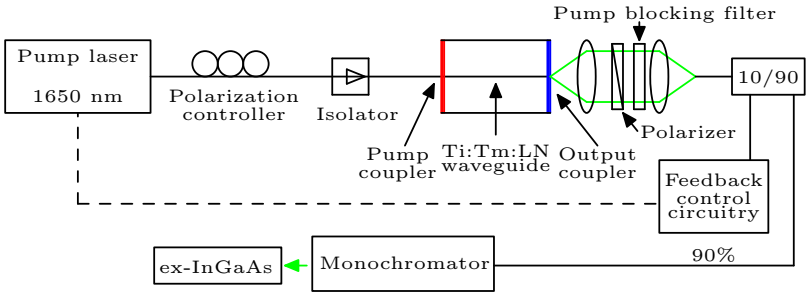

Figure 4.2: Experimental setup used to investigate the 30 mm long Ti:Tm:$LiNbO_3$ waveguide laser.

4.4 POWER CHARACTERISTICS

4.4.1 *High-Q Operation at λ_s = 1890 nm*

Laser emission was found near 1890 nm in TE-polarization only irrespective of the pump polarization. Fig. 4.3 presents the measured power characteristics for TE and TM polarized pump in cw operation (?). The laser output consisted of undamped relaxation oscillations was smoothed by a filter with a bandwidth of 22 Hz, for this measurement. The experimental setup described above was modified in such a way that the total laser output power (i.e., without spectral dispersion behind the waveguide) was measured. Lasing sets in at 6 mW of incident pump power corresponding to about 4 mW of cou-

pled pump power[1] only. With increasing pump power the spectrum of the pump laser shifts to somewhat longer emission wavelengths resulting in an even better pump absorption (see also Fig. 2.7). The result is a slightly increasing slope efficiency up to 13.3% at 38 mW coupled pump power. The output power of up to 4.5 mW (limited by the available pump power) was stable over time (Fig. 4.4.3).Both, the output power of the laser and the slope efficiency surpass the results reported so far for Tm:$LiNbO_3$ waveguide lasers [16, 17] by an order of magnitude.

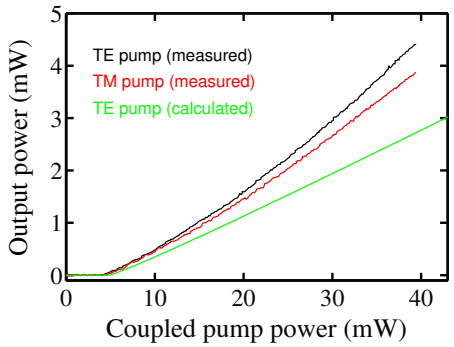

Figure 4.3: Measured power characteristics of the Ti:Tm:$LiNbO_3$ waveguide laser as output power (TE-polarization) versus coupled pump power in TE- and TM-polarization, respectively. In addition, a calculated characteristics is presented as output power versus coupled pump power for the laser emission wavelength of 1890 nm.

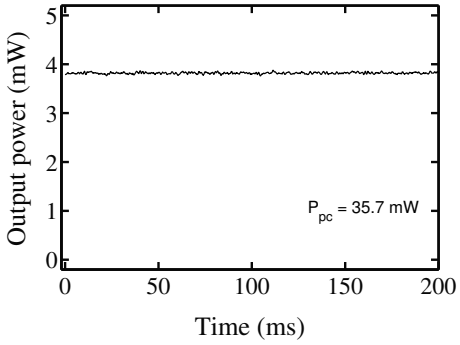

Figure 4.4: The laser output power, measured with ~1 kHz bandwidth, versus time.

A low threshold for the long wavelength emission can also be expected from qualitative arguments: due to the quasi four level system exploited, a low pump power is sufficient to get optical gain as already discussed in section 3.2.1 (see also section 3.3.3). Therefore, in a high-Q cavity lasing will start at that wavelength where the gain

1 66% coupling efficiency is assumed.

surpasses the overall losses first, when the coupled pump power is increased.

The power characteristics have also been modeled. As input parameters all the measured and derived data were used, which have been discussed above (waveguide propagation losses, mode distributions, absorption and emission cross sections, lifetimes of energy levels). In the case of laser we have endface mirrors and consequently R P Fiber Power can implement the relevant boundary conditions and calculate the optical gain arising from multiple round trips by the optical beam through the cavity, so that laser action can be simulated. Surprisingly, the modeling results show a somewhat larger threshold and a smaller slope efficiency than the experiments. We attribute this discrepancy to the calculated emission cross sections, which seem to be too small at the long wavelength side. The green curve shown in Fig. 4.3 is calculated with waveguide propagation loss coefficient of 0.1 dB/cm. The agreement becomes better (without a change in threshold pump power) when the calculation is done with waveguide propagation loss coefficient kept at 0.07 dB/cm.

4.4.2 *Low-Q Operation at λ_s = 1850 nm*

The laser wavelength could be shifted to 1850 nm by inducing additional losses into the cavity (described in detail in section 4.5.3). The corresponding power characteritics are given in Fig. 4.5. By the increased cavity losses the (coupled) threshold power was increased to ~ 9 mW and the slope efficiency of the laser characteristic was reduced to ~ 2.6%.

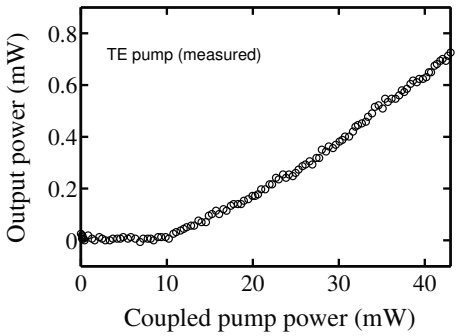

Figure 4.5: Measured power characteristics of the Ti:Tm:$LiNbO_3$ waveguide laser (λ_s = 1850 nm) as output power (TE-polarization) versus coupled pump power in TE polarization.

4.4.3 *Relaxation Oscillations*

As mentioned above, the laser output at both pump polarizations consisted of regular undamped relaxation spikings. Typical laser output at 50 mW incident pump power is shown in Fig. 4.6 (measurement bandwidth ~ 10 MHz). The left subfigure shows a regular pulse

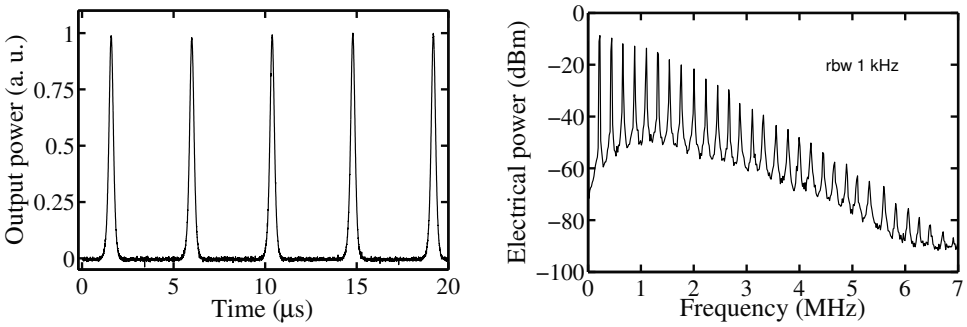

Figure 4.6: Output power of Ti:Tm:$LiNbO_3$ waveguide laser (λ_s = 1890 nm) for an incident power of 50 mW in time (left) and frequency (right) domains (measurement bandwidth > 10 MHz).

train with a repetiton frequency of 227 kHz and ~ 6% dutycycle. The right side figure shows the corresponding measurement in frequency domain, where several harmonics of the fundamental frequency are clearly visible. It has already been demonstrated that by opto-electronic feedback controlled pumping, such relaxation oscillations could be suppressed [40, 41]. A special example is the feed back controlled pumping of actively mode locked Ti:Er:$LiNbO_3$ waveguide laser[42]. In order to suppress the relaxation spikings of the Ti:Tm:$LiNbO_3$ laser, the same controlled pumping scheme was used. With this scheme, the peak corresponding to the fundamental relaxation oscillation frequency could be suppressed by more than 40 dB. This result is shown in Fig.4.7 (left). In this case, the incident pump power was only 14 mW. Fig. 4.7 (right) shows the integrated laser output power (without wavelength dispersion) recorded as a function of time. As evident from the figure, the laser out power was found to be stable over time, as it was shown before (see Fig.) with additional smoothing. On the other hand when the emission was wavelength dispersed with the monochromator, the relaxation spikings were observed to be irregular (see Fig. 4.8). This observation would mean that the gain experienced by different laser cavity modes are changing as a function of time eventhough the total laser output power remains stable. This observation fits well with the constant fluctuations recorded in the optical spectra (see section 4.5).

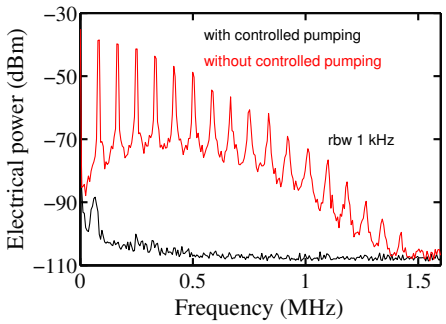

Figure 4.7: Laser output power in the frequency domain for 14 mW incident pump power with and without feedback controlled pumping. The frequency spectrum was measured with a resolution bandwidth (rbw) of 1 kHz.

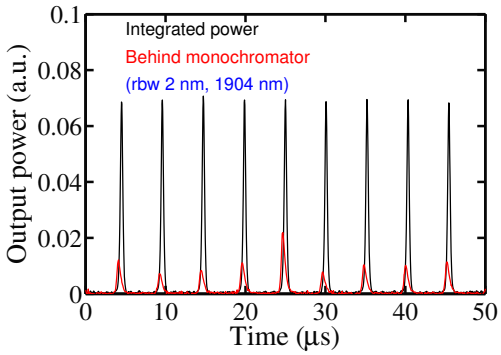

Figure 4.8: Output power of Ti:Tm:$LiNbO_3$ waveguide laser (λ_s = 1890 nm) in time domain: comparison between integrated output and spectrally resolved output centered at 1904 nm (resolution bandwidth 2 nm).

4.5 SPECTRAL PROPERTIES

4.5.1 *Emission at 1890 nm*

Laser emission spectra were measured with a monochromator of 250 pm resolution (measured independently with a line from extended cavity laser). The output from the photodiode (kept behind the monochromator) was recorded with a storage oscilloscope (measurement bandwidth ~ 53 kHz) while the monochromator was scanned in steps of 140 pm. The acquisition time at each data point was 2 s. In order to minimize the influence of water vapour absorption lines, the monochromator was purged with nitrogen. Irrespective of the pump polarization, the laser emission was found to be near 1890 nm and TE polarized. The fine structure of the laser spectra changed from scan to scan and was also found to be pump power dependent. Fig. 4.9 (left) shows as example the optical spectrum for TE polarized pump

at 32 mW incident pump power. The envelopes of the optical spectra were found to be (i) few nm wide, (ii) a function of pump power and (iii) changing from scan to scan. At higher pump power levels, the envelope of the spectrum became wider. An example is shown in Fig. 4.9 (right).

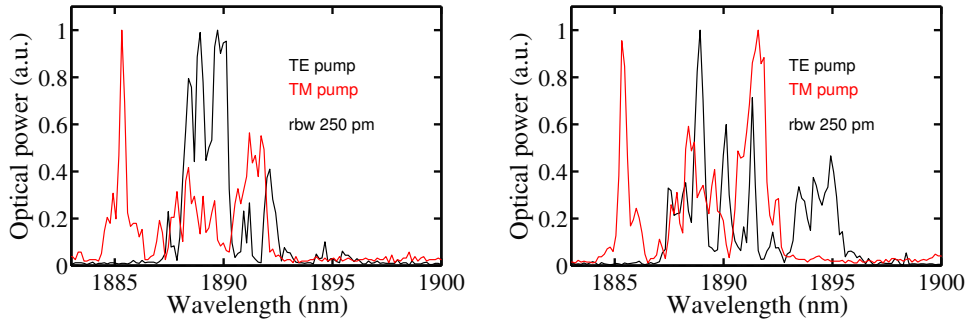

Figure 4.9: Measured optical spectra of Ti:Tm:$LiNbO_3$ waveguide laser (TE polarization; taken with a resolution bandwidth (rbw) of 250 pm) with emission near 1890 nm (high-Q cavity) for an incident power of 32 mW (left) and 51 mW (right).

Lasing at the longer wavelength side of the Tm emission spectrum can be understood by considering a four level system, i.e., pumping of atoms at the lower levels of the ground state multiplet to the higher lying levels of the excited state mutiplet and emission from the lower levels of the excited state multiplet to the high lying levels of the ground state multiplet. Due to thermalisation, the higher levels of both multiplets are rapidly depopulated to their low levels. As there are no wavelength selecting components inside the cavity and as the propagation losses of the waveguide are small, the gain achieved by longer wavelengths in the Tm emission spectrum, although low, is already sufficient to overcome the losses of the cavity and lasing action sets in.

4.5.2 *Radio Frequency Spectrum of Laser Output*

The radio frequency spectrum of the laser (λ_s=1890 nm) was recorded by a fast detector. The measurement result is shown in Fig. 4.10. Beat frequencies due to mode beating of longitudinal modes up to 8.8 GHz (free spectral range = 2.2 GHz) is clearly visible. Due to the broad optical spectrum, we can expect a large number of such beat frequency lines in the spectrum.

4.5.3 *Emission at 1850 nm*

By the integration of a tuneable wavelength filter into the cavity, a tuneable laser could be developed exploiting the large bandwidth of

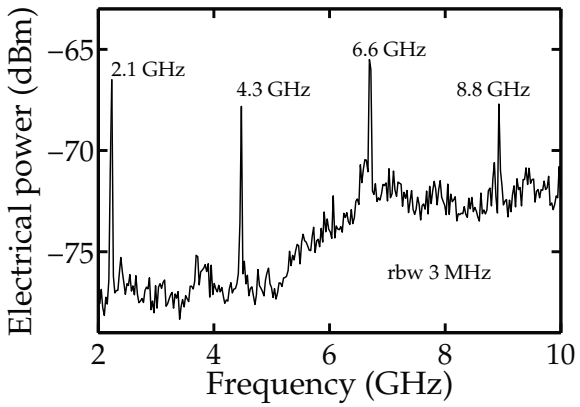

Figure 4.10: Measured electronic power spectrum of Ti:Tm:$LiNbO_3$ laser.

the gain (see Fig. 4.12). This approach has already been realized for Er-doped waveguide lasers using an acousto-optical filter [43]. For our Tm-doped laser, however, it would require the fabrication of another, more complicated device, which is an attractive challenge for the future. On the other hand, "tuneability" of the present device was demonstrated in quite a different way. By inducing additional losses in the cavity, the laser emission wavelength jumped to the neighbouring gain peak at ~ 1850 nm wavelength. This has been done by depositing a layer of silver paste on the waveguide surface. In this way additional propagation losses are induced by (partial) absorption of the evanescent tail of the laser mode in the metallic silver layer. Consequently, a higher gain is required to compensate the round trip propagation losses. However, by increasing the pump power, the required threshold gain cannot be achieved at ~ 1890 nm as in the high-Q cavity, but only at ~ 1850 nm, where laser emission sets in. A corresponding emission spectrum is shown in Fig. 4.12. By the increased cavity losses the (coupled) threshold power was increased to ~ 9 mW and the slope efficiency of the laser characteristic was reduced to ~ 2.6%.

Emission at the long wavelength side of the Tm $^3F_4 \rightarrow {}^3H_6$ transitions qualitatively explains the low threshold of the laser in case of a high Q cavity. However, it does not explain the fine structure of the observed emission spectrum, which should ideally consist of a single line (single longitudinal mode emission), if a homogeneously broadened laser material is used. Therefore, our conclusion is that a significant inhomogeneous broadening has been induced by the laser fabrication processes yielding concentration profiles of both, Tm and Ti ions. Moreover, spatial hole burning and small photorefractive effects might contribute to mode coupling and in this way to a time-varying broadening of the emission spectra. Nevertheless, we are confident that single mode emission can be achieved by appro-

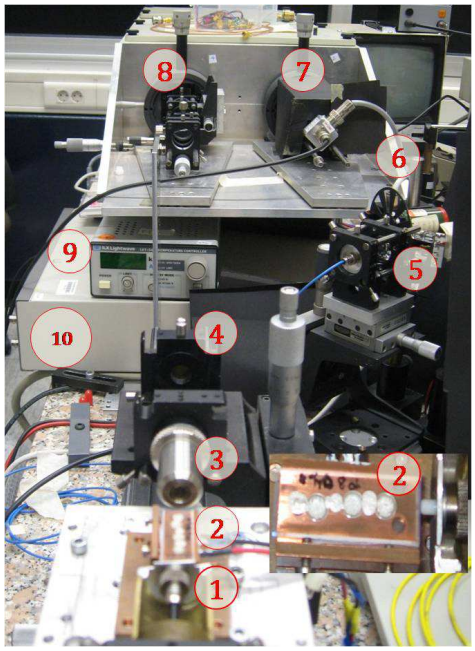

Figure 4.11: Experimental setup used to study the Ti:Tm:$LiNbO_3$ laser (λ_s=1850 nm). The waveguide laser 'covered' with silver paste is shown in inset also. The different components in the setup are 1: pump input fiber, 2: waveguide laser, 3: collimating lens behind the output coupler mirror of the laser, 4: pump blocking filter, 8: input side of the monochromator, 7: cooled ex-InGaAs photodiode at the output side of the monochromator and 9: current source for thermo-electric cooler of ex-InGaAs photodiode. In addition, the white light source (5) chopper (6) and lock-in amplifier (10) used in gain measurements are also visible in the photograph (see section 3.4).

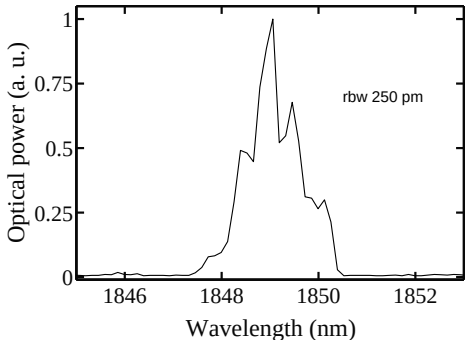

Figure 4.12: Measured optical spectrum (TE polarization; taken with a resolution bandwidth (rbw) of 250 pm) of the Ti:Tm:$LiNbO_3$ waveguide laser with emission near 1850 nm (low-Q cavity).

priate narrow-band spectral filtering as demonstrated for Er doped waveguide lasers [9].

	Southampton [16]	Madrid [17]	Paderborn
Gain Medium	Ti:Tm:$LiNbO_3$	Zn:Tm:$LiNbO_3$	Ti:Tm:$LiNbO_3$
$\lambda_{emission}$	1800 nm, 1850 nm	1762 nm	1890 nm, 1850 nm
λ_{pump}	795 nm	795 nm	1650 nm
Threshold	67 mW (launched)	34 mW (launched)	6 mW (incident)
Slope Efficiency	0.8%	1%	10%

Table 4.1: Comparison of different laser parameters of integrated Tm:$LiNbO_3$ lasers reported so far with those of the lasers reported in this thesis.

Table 4.1 gives a comparison of different laser parameters of integrated Tm:$LiNbO_3$ lasers reported so far with those of the lasers reported in this thesis.

4.6 OPTIMIZATION

In order to find the best combination of mirrors and waveguide length yielding maximum output power (and slope efficiency) for our double pass pumping scheme and emission at 1890 nm wavelength, additional simulations were performed. The results are presented in Fig. 4.13 as calculated output power (λ = 1890 nm) of the 3 cm long waveguide laser versus coupled pump power and in Fig. 4.14 versus device length (P_{pc} = 50 mW) with signal reflectivity R_{so} of the rear mirror (output coupler) as parameter. It is evident that the highest reflectivity results in the lowest threshold, but also in the lowest slope efficiency, η_{slope}. Reducing R_{so} increases the threshold, but increases the slope efficiency as well. With 50 mW coupled pump power the maximum laser output power of 14.5 mW is achieved with a mirror reflectivity of R_{so} = 80% (assuming that the resulting higher cavity loss will not yet induce a jump of the emission to a shorter wavelength; otherwise, a wavelength filter has to be incorporated). A further decrease of R_{so} reduces the output power again; only somewhat longer structures are a bit more efficient (not shown in Fig. 4.14 for reasons of clarity). The results presented in Fig. 4.14 confirm, that the chosen length of our waveguide laser of 3 cm is very close to the optimum choice. On the other hand, the mirror reflectivity of R_{so} = 98% of the fabricated device yields a low threshold, but not the maximum output power nor slope efficiency (green characteristic in Fig. 4.13). A significant optimization could be achieved with R_{so} = 80% instead of R_{so} = 98%: the slope efficiency would grow by a factor of four and nearly the same can be expected by the maximum output power (black characteristic in Fig. 4.13). And a reduction of the waveguide scattering losses (0.1 dB/cm have been assumed) and in this way of the cavity round trip losses would contribute to a further improvement of the laser.

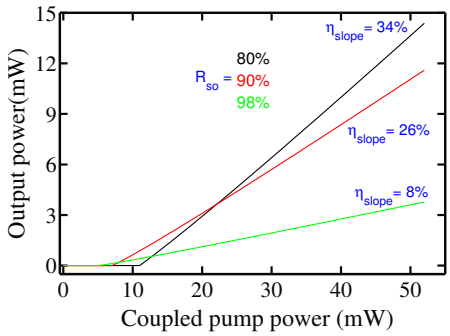

Figure 4.13: Calculated output power (λ = 1890 nm) of the Ti:Tm:$LiNbO_3$ waveguide laser (l = 3 cm) versus coupled pump power. The signal (pump) reflectivity of the input mirror is R_{si} = 90% (R_{pi} = 6%); the pump reflectivity of the output coupler is R_{po} = 96%.

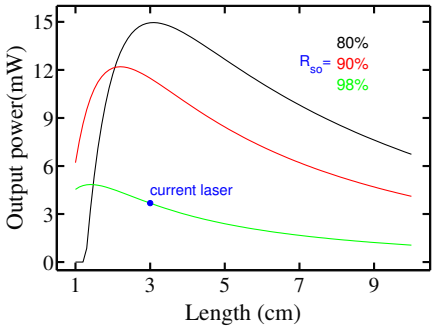

Figure 4.14: Calculated output power (λ = 1890 nm) of the Ti:Tm:$LiNbO_3$ waveguide laser (l = 3 cm) versus device length (P_{pc} = 50 mW) with signal reflectivity R_{so} of the rear mirror (output coupler) as parameter. The signal (pump) reflectivity of the input mirror is R_{si} = 90% (R_{pi} = 6%); the pump reflectivity of the output coupler is R_{po} = 96%.

An optimization for another emission wavelength and/or pump power level would result in a modified mirror reflectivity and device length. Moreover, it would require a wavelength selective component inside the cavity.

4.7 CONCLUSIONS

The 30 mm long free running laser (without wavelength selective components in the cavity) emits at 1890 nm, the longest emission wavelength of a Tm:$LiNbO_3$ laser reported so far; also 1850 nm emission could be demonstrated by increasing cavity losses. Laser threshold (1890 nm) of the double pass pumped device is ~4 mW coupled pump power only; the slope efficiency is ~11% resulting in a stable output power of ~4 mW, if pumped with ~40 mW (coupled power). Extensive modeling also demonstrates the potential of the laser: both, slope

efficiency and maximum output power should grow by about a factor of four by adjusting the reflectivity of the output mirror to ~80%.

5

CONCLUSIONS AND OUTLOOK

5.1 CONCLUSIONS

The fabrication of Ti:Tm:Li:NbO_3 waveguide by diffusion doping is briefly described. The characterization of the waveguide by means of scattering loss and near field measurements are subsequently discussed. The experimental studies of the properties of the waveguide due to Tm doping (absorption and fluorescence spectra) are also presented. The transition cross sections of the Tm-doped waveguide which are important from the point of view of amplifier/laser fabrication using the waveguide were determined for the first time using the McCumber theory.

In-band pumping using 1660 nm laser radiation was found to be the optimum for pumping the experimentally studied waveguide amplifier and laser discussed in this thesis. Modeling results demonstrate that broad-band optical gain in the wavelength range 1750 nm $< \lambda_s <$ 1900 nm can be achieved using the Ti:Tm:$LiNbO_3$ waveguide as an amplifier, when pumped at 1650 nm. Results of small signal gain measurements are found to be in good agreement with the corresponding modeling results for the case of single pass pumping scheme. Modeling results point to the possibility to achieve (wavelength dependent) gain of upto 30 dB from a 10 cm long single pass pumped waveguide. The gain achieveable with a given pump power level can be improved by implementing double pass pumping along with a careful choice of waveguide length. Such double pass pumped amplifiers can be used to realize waveguide lasers operating at any wavelength in the broadband signal spectrum where optical gain can be achieved.

The 30 mm long free running laser (without wavelength selective components in the cavity) realized using a Ti:Tm:Li:NbO_3 waveguide with dielectric mirrors deposited at the waveguide endfaces emits at 1890 nm, the longest emission wavelength of a Tm:$LiNbO_3$ laser reported so far; also 1850 nm emission could be demonstrated by increasing cavity losses. Laser threshold (1890 nm) of the double pass pumped device is ~4 mW coupled pump power only; the slope efficiency is ~11% resulting in a stable output power of ~4 mW, if pumped with ~40 mW (coupled power). Extensive modeling also demonstrates the potential of the laser: both, slope efficiency and maximum output power should grow by about a factor of four by adjusting the reflectivity of the output mirror to ~80%.

It should be possible to realize a whole family of lasers using the Ti:Tm:$LiNbO_3$ waveguide as the family of Ti:Er:$LiNbO_3$ waveguide lasers demonstrated in the past[9]. An exciting possibility which has not yet been realized in the case of Ti:Er:$LiNbO_3$ lasers is the demonstration of a passively mode-locked laser. This can be done by coating a layer of carbon nanotube (CNT) on top of the waveguide, so that the CNT layer interacts with the evanescent tail of the laser field as a saturable absorber, leading to mode-locking. The 1850 nm laser demonstrated in this thesis shows the potential of this approach. This has already been realized in the case of fiber lasers. Another approach is to use a suitably designed semiconductor saturable absorber mirror butted at one of the endfaces to form the laser cavity.

A

THULIUM DOPED WAVEGUIDES FOR QUANTUM MEMORY APPLICATIONS

A.1 WAVEGUIDE FABRICATION

Commercially available 0.5 mm thick Z-cut wafers of undoped optical grade congruent lithium niobate (CLN) were used as starting material. Samples of 12 mm x 30 mm size were cut from these wafers and doped by thulium near the +Z-surface before waveguide fabrication. The doping was achieved by in-diffusing a vacuum deposited (electron-beam evaporated) Tm layer of 19.6 nm thickness. The diffusion was performed at 1130°C during 150 h in an argon-atmosphere followed by a post treatment in oxygen (1 h) to get a full re-oxidization of the crystal.

To determine the diffusion coefficient of Tm into Z-cut CLN, secondary neutral mass spectroscopy (SNMS) was performed using 700 eV Argon-ions for ion milling. Ions and electrons were extracted from the plasma source with a duty cycle of 4:1 at a rate of 320 kHz to avoid charging of the insulating CLN-substrate. SNMS was chosen instead of secondary ion mass spectroscopy (SIMS) to significantly reduce matrix effects (see e.g. [27]). In Fig. A.1, the concentration profiles versus depth have been recorded for thulium (Tm), lithium (Li), niobium (Nb) and oxygen (O). Interestingly, the Li-concentration slightly increases towards the surface, although it is expected that Tm occupies regular Li-sites similar to Er-ions when incorporated in CLN by diffusion [28].

In Fig.A.2, the Tm concentration is plotted on a linear scale versus the depth. The slight dip close to the surface is unexpected and needs further investigations. Fitting a Gaussian profile to the concentration curve leads to a 1/e-penetration depth $d_{1/e}$ of about 6.5 µm.The max-

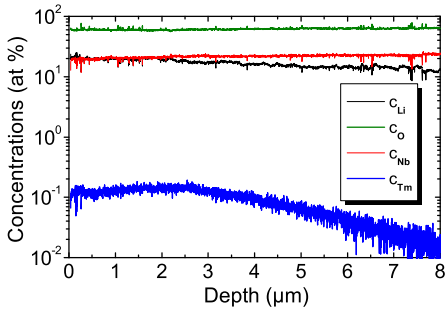

Figure A.1: Measured concentrations of Tm, Li, Nb, and O versus depth, using SNMS with 700 eV Ar-ions.

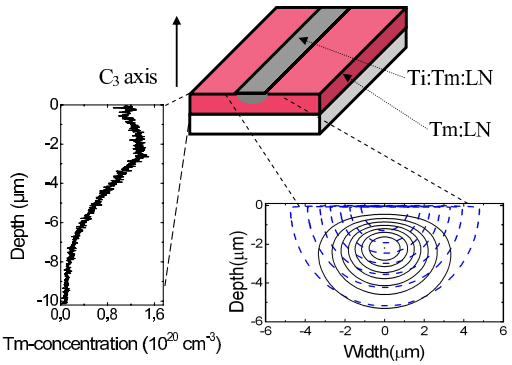

Figure A.2: Scheme of the waveguide geometry with the measured Tm concentration profile on the left and the calculated intensity distribution of the fundamental TM-mode superimposed on the profile of the extraordinary index of refraction induced by the Ti-doping. The latter data are for 795 nm wavelength. Iso-intensity lines are plotted for both, the index and the mode profile, corresponding to 100%, 87.5%, 75% etc. of the maximum index increase ($\Delta n_{max} = 4.0 \times 10^{-3}$) and mode intensity, respectively.

imum Tm concentration of about $1.35 \cdot 10^{20}$ cm^{-3} corresponds to a concentration 0.74 mole %, which - according to Ref. [28] - is considerably below the solid solubility of Tm in CLN.

On the Tm-diffusion doped surface of the substrate, a 40 nm thick titanium (Ti) layer was deposited using electron-beam evaporation. From this layer, 3.0 μm wide Ti stripes were photolithographically defined and subsequently in-diffused at 1060°C for 5 h to form 30 mm long optical strip waveguides. In the wavelength range around 775 nm, the waveguides are single mode for TE- and TM-polarization (see Fig. A.2).

The total waveguide propagation loss at room temperature, including absorption and scattering loss, were measured by the Fabry-Pérot method [26]. A stabilized, single frequency Ti:Sapphire laser was used to measure the transmission of the low-finesse waveguide resonator as function of a small temperature change at a number of fixed wavelengths in the range between 750 nm and 807 nm. From the contrast of the measured Fabry-Perot response, the propagation loss was deduced for all wavelengths. The results are presented in Fig. A.3 for TM-polarization. The waveguide propagation loss was determined at room temperature and 729 nm wavelength, where negligible absorption by the Tm-ions can be expected. Therefore, the measured loss coefficients reflect the scattering loss alone; it is 0.2 dB/cm for TE- as well as for TM-polarization. As the scattering loss is only weakly dependent on the wavelength, it can be regarded as a background for the Tm-induced absorption loss.

A.2 WAVEGUIDE CHARACTERIZATION

The transmission through a 30 mm long waveguide for TE and TM-polarized light is shown in Fig. A.3. It has been normalized to the incident spectral power density of the broadband tungsten lamp used in this experiment. We observe broad absorption, reflecting different transitions between Stark levels in the $^3H_6$ and $^3H_4$ multiplets superimposed with inhomogeneous broadening, and the thermal distribution of the population in the electronic ground state. In addition, a strong polarization dependence of absorption is observed, confirming previous studies performed on bulk crystals [44, 30].

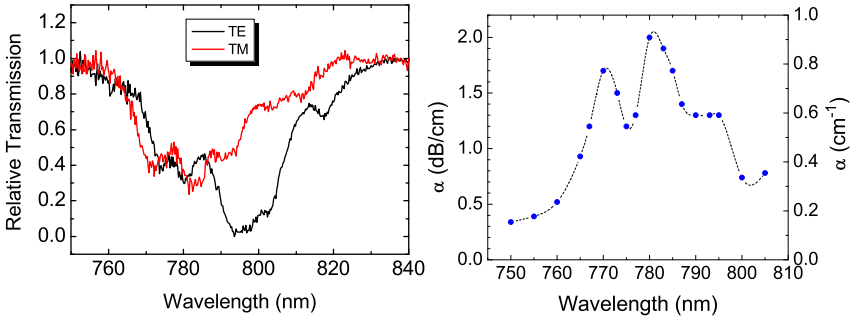

Figure A.3: Relative transmission through the Ti:Tm:$LiNbO_3$ waveguide for TM- and TE-polarization, respectively, as a function of wavelength (left figure). The resolution bandwidth of the optical spectrum analyzer used in this experiment was 2 nm due to the low spectral power density of the thermal radiator.Measured loss coefficient (α) for TM-polarization as a function of wavelength (right side). Data points are connected by spline fitting as a guide for the eye.

A.3 QUANTUM MEMORY

Our collaborators from the University of Calgary (Group of Prof.Tittel) made spectroscopic measurements of this sample at 4K[24] and subsequently succeeded in demonstrating the first waveguide quantum memory[13] with this sample.

B

OPTICAL SPECTRUM OF Ti:Er:$LiNbO_3$ WAVEGUIDE LASER

The optical spectrum of waveguide laser sample Pb149z (with endface mirrors on both endfaces) is presented below. The laser cavity was formed by mirrors similar to those described in [14]. The scattering losses the waveguide were estimated to be α_s = 0.03 dB/cm [1].

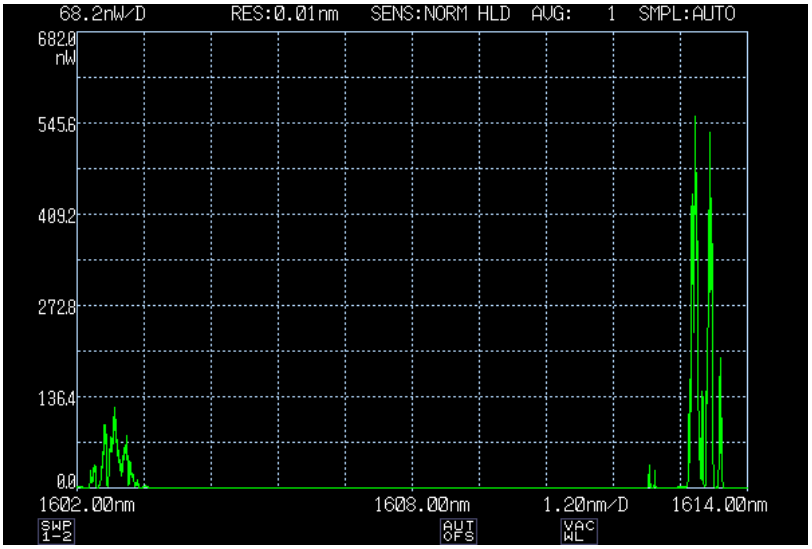

Figure B.1: Optical spectrum of self-pulsing Ti:Er:$LiNbO_3$ waveguide laser for TM polarized pumping at 1480 nm. The laser was lasing simultaneously at 1602 nm and 1614 nm.

1 Measurement done by Dr.Selim Reza.

6

ACKNOWLEDGEMENTS

First of all I would like thank Almighty God for all the never ending gracious blessings showered on my life.

I would like to thank the members of my Ph.D. commission Prof. Wolf Gero Schmidt (chairperson), Prof. Wolfgang Sohler (first reviewer), Prof. Donat As (second reviewer) and Dr. Simone Sanna (representative from scientific colleagues) for offering their service.

Prof. Sohler, my supervisor, gave me the invaluable opportunity to work in his group. His guidance and constant encouragement allowed me to reach higher levels of excellence which often I did not envisage when I started with something, an experiment for example. During the initial years of my stay in Paderborn, Selim Reza and Hubertus Suche helped me in getting familiar with the lab and the physics of various experiments in great detail. They helped me in fine tuning my skills in such a way that I can 'stand on my own'. Ms. Irmgard Zimmermann was always there to extend all the help and guidance with all official matters and even with advice on living at Paderborn, whenever it was sought. Harald Hermann was always generous in spending his time whenever an opinion or advice was sought about my doubts on various topics of my research. He extended his advice (in programming and) in getting the HR640 monochromator, which was kept idle for about 10 years, up and running practically from scratch. Prof. As was kind enough to provide the user manual of HR640 upon my request. Raimund Ricken helped me in getting all the samples prepared. Viktor Quiring prepared all the special mirrors and special coatings on sample end faces (and top surfaces) for me. Both Raimund and Viktor were always willing to extend a helping hand in getting things done by the mechanical workshop (often saving valuable time). My friends and former colleagues, Abu Thomas, Miguel Garcia Granda, Ansgar Hellwig, Hui Hu, Li Gui, Rahman Nouroozi, Sergey Orlov, Daniel Büchter, Dirk Mantei, Shantanu Pal, Kai-Huong Luo, Suhas Bhandare, Bhaskar Bhandarapu, Vitali Mirvoda, Ali Al-Bermani, Omar Jan, Benjamin Koch, Kidsanapong Puntsri and Xu Yang were always happy to lend a helping hand whenever asked for. Prof. Silberhorn and her group members extended all the support and encouragement they possibly could to enrich my stay at Paderborn. Prof. Noé and David Sandel always allowed me to use several of their laboratory equipments for my research. My discussions with Dr. Rüdiger Paschotta were often illuminating. I would like to extend my sincere gratitude to all of the above mentioned persons. Perhaps I have missed to in-

clude some of the people who have enriched my stay at Paderborn. Thanks to all of those as well.

I would like to to thank my parents and my wife for encouraging me although I was far away from them.

The financial support extended to me by the people of NRW (via a Ph.D. position), the people of the European Union (via QuRep project) and Deutsche Forchungsgemeinschaft (via GRK-1464) is gratefully acknowledged.

BIBLIOGRAPHY

[1] T. H. Maiman. Stimulated optical radiation in ruby. *Nature*, 187:493–515, 1960.

[2] Th. Udem, R. Holzwarth, and T. W. Hänsch. Optical frequency metrology. *Nature*, 416:233–237, 2002.

[3] Qian Peng, Asta Juzeniene, Jiyao Chen, Lars O Svaasand, Trond Warloe, Karl-Erik Giercksky, and Johan Moan. Lasers in medicine. *Reports on Progress in Physics*, 71(5):056701, 2008.

[4] Ginés Lifante. *Integrated Photonics*. Wiley VCH, 2003.

[5] S. E. Miller. Integrated optcs: An introduction. *The Bell System Technical Journal*, 48:2049–2069, 1969.

[6] C. Gunn. CMOS photonics for high-speed interconnects. *IEEE Micro*, 26(2):58 –66, march-april 2006.

[7] Western Bolanos, Joan J. Carvajal, Xavier Mateos, Ganapathy Senthil Murugan, Ananth Z. Subramanian, James S. Wilkinson, Eugenio Cantelar, Daniel Jaque, Ginés Lifante, Magdalena Aguiló, and Francisco Díaz. Mirrorless buried waveguide laser in monoclinic double tungstates fabricated by a novel combination of ion milling and liquid phase epitaxy. *Optics Express*, 18:26937–26945, 2010.

[8] Wolfgang Sohler, Hui Hu, Raimund Ricken, Viktor Quiring, Christoph Vannahme, Harald Herrmann, Daniel Büchter, Selim Reza, Werner Grundkötter, Sergey Orlov, Hubertus Suche, Rahman Nouroozi, and Yoohong Min. Integrated optical devices in lithium niobate. *Optics and Photonics News*, 19:24–31, 2008.

[9] W. Sohler, B. Das, D. Dey, S. Reza, H. Suche, and R. Ricken. Erbium-doped lithium niobate waveguide lasers. *IEICE Transactions Electron. E*, 88-C:990–997, 2005.

[10] Martin Hempstead, , James S. Wilkinson, and Laurence Reekie. Waveguide lasers operating at 1084 nm in neodymium-diffused lithium niobate. *IEEE Photonics Technology Letters*, 4(8):852–855, 1992.

[11] E. Lallier, J.P. Pocholle, M. Papuchon, M.P. DeMicheli, M.J. Li, Q. He, D.B. Ostrowsky, C. Grezes-Besset, and E. Pelletier. Nd:MgO:$LiNbO_3$ channel waveguide laser devices. *IEEE Journal of Quantum Electronics*, 27(3):618–625, 1991.

[12] R. Brinkmann, I. Baumann, M. Dinand, W. Sohler, and H. Suche. Erbium-doped single- and double-pass Ti:$LiNbO_3$ waveguide amplifiers. *IEEE Journal of Quantum Electronics*, 30(10):2356 –2360, 1994.

[13] Erhan Saglamyurek, Neil Sinclair, Jeongwan Jin, Joshua A. Slater, Daniel Oblak, Félix Bussiéres, Mathew George, Raimund Ricken, Wolfgang Sohler, and Wolfgang Tittel. Broadband waveguide quantum memory for entangled photons. *Nature*, 469:512–515, 2011.

[14] Mathew George, Selim Reza, Hubertus Suche, Raimund Ricken, and Viktor Quiring Wolfgang Sohler. Self-pulsing Ti:Er:$LiNbO_3$ waveguide laser. In *European Conference on Lasers and Electro-Optics 2009 and the European Quantum Electronics Conference. CLEO Europe - EQEC 2009.*, 2009.

[15] Alphan Sennaroglu, editor. *Solid-State Lasers and Applications*. CRC Press, 2006.

[16] de Sandro J.P., Jones J.K., Shepherd D.P., Hempstead M., J. Wang, and Tropper A.C. Non-photorefractive CW Tm-indiffused Ti:$LiNbO_3$ waveguide laser operating at room temperature. *IEEE Photonics Technology Letters*, 8(2):209–211, 1996.

[17] E. Cantelar, J. A. Sanz-Garcia, G. Lifante, F. Cussó, and P. L. Pernas. Single polarized Tm^{3+} laser in Zn-diffused $LiNbO_3$ channel waveguides. *Applied Physics Letters*, 86(16):161119, 2005.

[18] D. G. Lancaster, S. Gross, H. Ebendorff-Heidepriem, A. Fuerbach, M. J. Withford, and T. M. Monro. 2.1 μm waveguide laser fabricated by femtosecond laser direct-writing in Ho3+, Tm3+:ZBLAN glass. *Optics Letters*, 37(6):996–998, 2012.

[19] S. Rivier, X. Mateos, V. Petrov, U. Griebner, Y. E. Romanyuk, C. N. Borca, F. Gardillou, and M. Pollnau. Tm:$KY(WO_4)_2$ waveguide laser. *Optics Express*, 9:5885–5892.

[20] I. Baumann, S. Bosso, R. Brinkmann, R. Corsini, M. Dinand, A. Greiner, K. Schäfer, J. Söchtig, W. Sohler, H. Suche, and R. Wessel. Er-doped integrated optical devices in $LiNbO_3$. *IEEE Journal of Selected Topics in Quantum Electronics*, 2:355–366, 1997.

[21] I. Baumann, R. Brinkmann, M. Dinand, W. Sohler, L. Beckers, Ch. Buchal, M. Fleuster, H. Holzbrecher, H. Paulus, K.-H. Müller, Th. Gog, G. Materlik, O. Witte, H. Stolz, and W. von der Osten. Erbium incorporation in $LiNbO_3$ by diffusion-doping. *Applied Physics A*, 64:33–44, 1997.

[22] I. Baumann, F. Cussó, B. Herreros, H. Holzbrecher, H. Paulus, K. Schäfer, and W. Sohler. Praseodymium-doped Ti:$LiNbO_3$ waveguides. *Applied Physics A*, 68:321–324, 199.

[23] Mathew George, Raimund Ricken, Wolfgang Sohler, E. Saglamyurek, N. Sinclair, C. La Mela, and W. Tittel. Ti:Tm:$LiNbO_3$ waveguide for quantum memory applications. In *European Conference on Integrated Optics*, 2010.

[24] N. Sinclair, E. Saglamyurek, M. George, R. Ricken, C. La Mela, W. Sohler, and W. Tittel. Spectroscopic investigations of a Ti:Tm:$LiNbO_3$ waveguide for photon-echo quantum memory. *Journal of Luminescence*, 130:1586 – 1593, 2010.

[25] Strake E., Bava G.P., and Montrosset I. Guided modes of Ti:$LiNbO_3$ channel waveguides: a novel quasi-analytical technique in comparison with the scalar finite-element method. *IEEE Journal of Lightwave Technology*, 6(6):1126 –1135, 1988.

[26] R. Regener and W. Sohler. Loss in low-finesse Ti:$LiNbO_3$ optical waveguide resonators. *Applied Physics B*, 36:143–147, 1985.

[27] H. Bubert and H. Jenett (eds.). *Surface and Thin Film Analysis*. Wiley, 2002.

[28] M. Quintanilla, E. Cantelar, J.A. Sanz-García, and F. Cussó. Growth and optical characterization of Tm^{3+}-doped $LiNbO_3$. *Optical Materials*, 30:1098 – 1102, 2008.

[29] E. Cantelar, G. Lifante, and F. Cussó. Modelling of Tm^{3+} doped $LiNbO_3$ waveguide lasers. *Optical and Quantum Electronics*, 38:111–122, 2006.

[30] E. Cantelar, M. Quintanilla, P.L. Pernas, G.A. Torchia, G. Lifante, and Cussó. Polarized emission and absorption cross-section calculation in $LiNbO_3$:Tm^{3+}. *Journal of Luminescence*, 128:988 – 991, 2008.

[31] P. C. Becker, N. A. Olsson, and J R Simpson. *Erbium Doped Fiber Amplifiers, Fundamentals and Technology*. Academic Press, 1999.

[32] Rodica. M. Martin. *Reciprocity between emission and absorption for rare earth ions in glass - Ph.D. thesis*. Worcester Polytechnic Institute, 2006.

[33] M.J.F. Digonnet, E. Murphy-Chutorian, and D.G. Falquier. Fundamental limitations of the McCumber relation applied to Er-doped silica and other amorphous-host lasers. *IEEE Journal of Quantum Electronics*, 38(12):1629 – 1637, 2002.

[34] Joseph T. Verdeyen. *Laser Electronics*. Prentice Hall, 2 edition, 1989.

[35] Yong Wang, Deyuan Shen, Hao Chen, Jian Zhang, Xianpeng Qin, Dingyuan Tang, Xiaofang Yang, and Ting Zhao. Highly efficient Tm:YAG ceramic laser resonantly pumped at 1617 nm. *Optics Letters*, 36:4485–4487, 2011.

[36] R. Brinkmann, I. Baumann, M. Dinand, W. Sohler, and H. Suche. Erbium-doped single- and double-pass Ti:$LiNbO_3$ waveguide amplifiers. *IEEE Journal of Quantum Electronics*, 30:2356–2360, 1994.

[37] R P Photonics Consulting GmbH. www.rp-photonics.com.

[38] R P Fiber Power V 3.0 - User Manual. pages 14 – 15.

[39] Marc Eichhorn. High-gain Tm-doped fluoride fiber amplifier. *Optics Letters*, 30:456–458, 2005.

[40] S. Valling, B. Ståhlberg, and Å.M. Lindberg. Tunable feedback loop for suppression of relaxation oscillations in a diode-pumped Nd:YVO_4 laser. *Optics and Laser Technology*, 39(1):82 – 85, 2007.

[41] S. Taccheo, P. Laporta, O. Svelto, and G. De Geronimo. Intensity noise reduction in a single-frequency ytterbium-codoped erbium laser. *Optics Letters*, 21:1747–1749, 1996.

[42] Rudolf Wessel. *Actively Mode Locked Waveguide Lasers in Erbium Doped Lithium Niobate, Ph.D. thesis*. 2003.

[43] K. K. Schäfer, I. Baumann, W. Sohler, H. Suche, and S. Westenhöfer. Diode-pumped and packaged acoustooptically tunable Ti:Er:$LiNbO_3$ waveguide laser of wide tuning range. *IEEE Journal of Quantum Electronics*, 33(10):1636 –1641, 1997.

[44] L. Núñez, J. O. Tocho, J. A. Sanz-García, E. Rodríguez, F. Cussó, D.C. Hanna, A.C. Tropper, and A.C. Large. Optical absorption and luminescence of Tm^{3+}-doped $LiNbO_3$ and $LiNbO_3$(MgO) crystals. *Journal of Luminescence*, 55:253 – 263, 1993.